ISSN 0036-0236, Russian Journal of Inorganic Chemistry, 2014, Vol. 59, No. 12, pp. 1361–1382. © Pleiades Publishing, Ltd., 2014.
Original Russian Text © V.G. Sevastyanov, E.P. Simonenko, A.N. Gordeev, N.P. Simonenko, A.F. Kolesnikov, E.K. Papynov, O.O. Shichalin, V.A. Avramenko, N.T. Kuznetsov, 2014, published in Zhurnal Neorganicheskoi Khimii, 2014, Vol. 59, No. 12, pp. 1611–1632.

SYNTHESIS AND PROPERTIES OF INORGANIC COMPOUNDS

HfB_2-SiC (10–20 vol %) Ceramic Materials: Manufacture and Behavior under Long-Term Exposure to Dissociated Air Streams

V. G. Sevastyanov[a], E. P. Simonenko[a, b], A. N. Gordeev[c], N. P. Simonenko[a], A. F. Kolesnikov[c], E. K. Papynov[d, e], O. O. Shichalin[d, e], V. A. Avramenko[d, e], and N. T. Kuznetsov[a]

[a] *Kurnakov Institute of General and Inorganic Chemistry, Russian Academy of Sciences, Leninskii pr. 31, Moscow, 119991 Russia*
e-mail: ep_simonenko@mail.ru
[b] *Lomonosov Moscow State University of Fine Chemical Technologies, pr. Vernadskogo 86, Moscow, 119571, Russia*
[c] *Ishlinskii Institute for Problems in Mechanics, Russian Academy of Sciences, pr. Vernadskogo 101, block 1, Moscow, 119526 Russia*
[d] *Institute of Chemistry, Far-East Branch, Russian Academy of Sciences, pr. Stoletiya Vladivostoka 159, Vladivostok, 690022, Russia*
[e] *Far-Eastern Federal University, ul. Sukhanova 8, Vladivostok, 690950 Russia*

Received June 14, 2014

Abstract—Ultra-high-temperature composite materials HfB_2-SiC containing 10, 15, and 20 vol % SiC were prepared by spark plasma sintering. The behavior of the samples prepared under long-term exposure to subsonic dissociated airstreams of a high-frequency induction plasmatron was studied. The total test time per sample was 35–42 min. Under certain exposure conditions (which were dependent on the composition of a sample), some regions of the sample were found to experience a rapid increase in temperature up to 2700°C. These regions enlarged over time, so that most of the surface area of the sample experienced exposure to temperatures of up to 2500–2700°C for 19–38 min, while the rest of the surface had a temperature of up to 1800–1900°C during almost the entire duration of the experiment. The joint use of optical microscopy, scanning electron microscopy (with EDX analysis), and X-ray powder diffraction enabled us to study the microstructure and composition of a structurally complex oxidized layer.

DOI: 10.1134/S0036023614120250

Ceramic composites based on zirconium or hafnium diborides and silicon carbide (ZrB_2-SiC and HfB_2-SiC, in particular when doped with other components) are advanced by many researchers as promising materials for use in the design of thermally loaded parts, in particular, nose cones and sharp edges of wings in hypersonic aircrafts [1–7]. Due to the lucky combination of properties such as high melting temperatures and nonexistence of phase transitions, resistance to oxidation in air due to the ability to form a borosilicate glass barrier layer, and high heat conductivity (in particular at high temperatures), the aforementioned ceramic materials are capable of withstanding heating to temperatures higher than 2000°C under exposure to dissociated air streams [6–10]. The dopant silicon carbide plays an important role in these materials, and this implies that the silicon carbide percentage and distribution in the material are also of great importance in the context of oxidation stability and functional characteristics on the whole. The most recommended composites comprise 10 to 30 vol % silicon carbide [11–23], although materials with higher silicon carbide percentages (of up to 45 vol % SiC) have recently been reported to be efficacious, in particular under exposure to high-enthalpy air flows [6, 7, 24, 25]. The most popular methods for manufacturing such materials are hot molding and spark plasma sintering at temperatures of 1900–2200°C; these methods make it possible to attain 98–100% densities of the calculated values and (as our colleagues suggest) would thereby improve the mechanical properties and oxidative resistance due to hindered oxygen diffusion. However, our earlier studies [6, 7] showed that relatively porous materials (where the calculated porosity was 19–30%) withstood long-term exposure to dissociated air flows at temperatures higher than 2000°C (up to 2700°C). We should mention that those studies were performed on a sample with a high silicon carbide percentage (25–45 vol %).

The goal of this study was to prepare HfB_2-SiC composite materials containing 10, 15, and 20 vol % silicon carbide and having relatively high porosities using spark plasma sintering and to study their behavior under long-term exposure to dissociated air flows at temperatures above 2000°C.

Table 1. Selected properties of HfB_2-SiC ceramic samples

Set	SiC percentage, vol %	Density, g/cm^3	Porosity*, %	Surface roughness parameters, μm	
				R_a**	R_y**
1 (HfB_2-10SiC)	10	6.7 ± 0.1	35.6 ± 1.0	1.7 ± 0.4	4.9 ± 1.1
2 (HfB_2-15SiC)	15	6.3 ± 0.1	39.7 ± 1.5	1.8 ± 0.4	5.0 ± 1.2
3 (HfB_2-20SiC)	20	6.8 ± 0.1	34.9 ± 1.0	1.3 ± 0.2	3.5 ± 0.4

* Determined compared to the additively calculated density values (the HfB_2 density is set equal to 10.5 g/cm^3 [27] and the SiC density to 3.2 g/cm^3 [28]).

** R_a is the arithmetic mean deviation of the profile; R_y is the maximal height of the profile as determined on the baseline length of 1.25 mm.

EXPERIMENTAL

The reagents used were hafnium diboride (pure grade; particle size: 2–3 μm; aggregate size: ~20–60 μm) and silicon carbide (pure grade; average particle size: 100 μm).

Samples were manufactured on an SPS-515S Spark Plasma Sintering System (from Dr.Sinter-LAB™) as follows: a premicronized mixture of HfB_2 and SiC powders (where SiC percentages were 10, 15, and 20 vol % for sets 1, 2, and 3, respectively) was placed into a graphite die, compacted, evacuated, and then sintered at a temperature below 1500°C under pressure and under exposure to electric pulses with an exposure time at the maximal temperature of 20 min. Cylinder-shaped samples (15 mm in diameter, ~5 mm high, and ~5 g in weight) were obtained in this way and were then polished.

Surface roughness parameters were determined using a TR200 (Time Group Inc.) portable roughness tester with a baseline length of 1.25 mm.

X-ray powder diffraction studies were carried out on a Bruker D8 Advance X-ray diffraction diffractometer (CuK_α radiation, 0.02° resolution).

IR transmission spectra were recorded as Nujol mulls in KBr plates on an FT-08 Infralum IR spectrometer.

Scanning electron microscopy (SEM) studies were performed on an NVision 40 (Carl Zeiss) triple-beam workstation; elemental microanalysis was carried out using an EDX Oxford Instruments energy-dispersive attachment.

Experiments where the sample surface was exposed to a subsonic stream of dissociated air were performed on a 100-kW VGU-4 high-frequency induction plasmatron [26], in the Institute for Problems in Mechanics, with an anode supply power of 45 to 72 kW and a pressure of 100 to 300 hPa. The surface temperature was measured with a Mikron M-770S pyrometer in the spectral ratio pyrometer mode (temperature range: 1000–3000°C; measurement spot size: ~5 mm). Temperature distribution over the front surface of the sample was determined using a Tandem VS-415U thermal imager.

RESULTS AND DISCUSSION

Characterization of Manufactured HfB_2-SiC Composite Materials

HfB_2-SiC ceramic samples containing 10, 15, and 20 vol % silicon carbide were manufactured by spark plasma sintering. Their apparent densities, calculated porosities, and roughness parameters are given in Table 1.

Noteworthy, the HfB_2-SiC ceramic samples containing high silicon carbide percentages (25–45 vol %) prepared earlier by a similar method had porosities of 20–32% [6, 7]. It follows that, provided similar manufacture parameters, a reduction in SiC percentage leads to higher porosities of the resulting samples, although 10 vol % silicon carbide samples poorly fit this trend because their porosities are close to those of samples containing 20 vol % SiC. Surface roughness measurements showed values close to those recommended in the literature, which are less than 1–2 μm as. The arithmetic mean deviation of the profile R_a determined on the baseline length of 1.25 mm was 1.7 ± 0.4 μm for samples of set 1 (with the minimal SiC percentage), and the maximal height of the profile R_y was ~5 μm, which slightly exceeds the required parameters. The surface roughness was reduced sys-

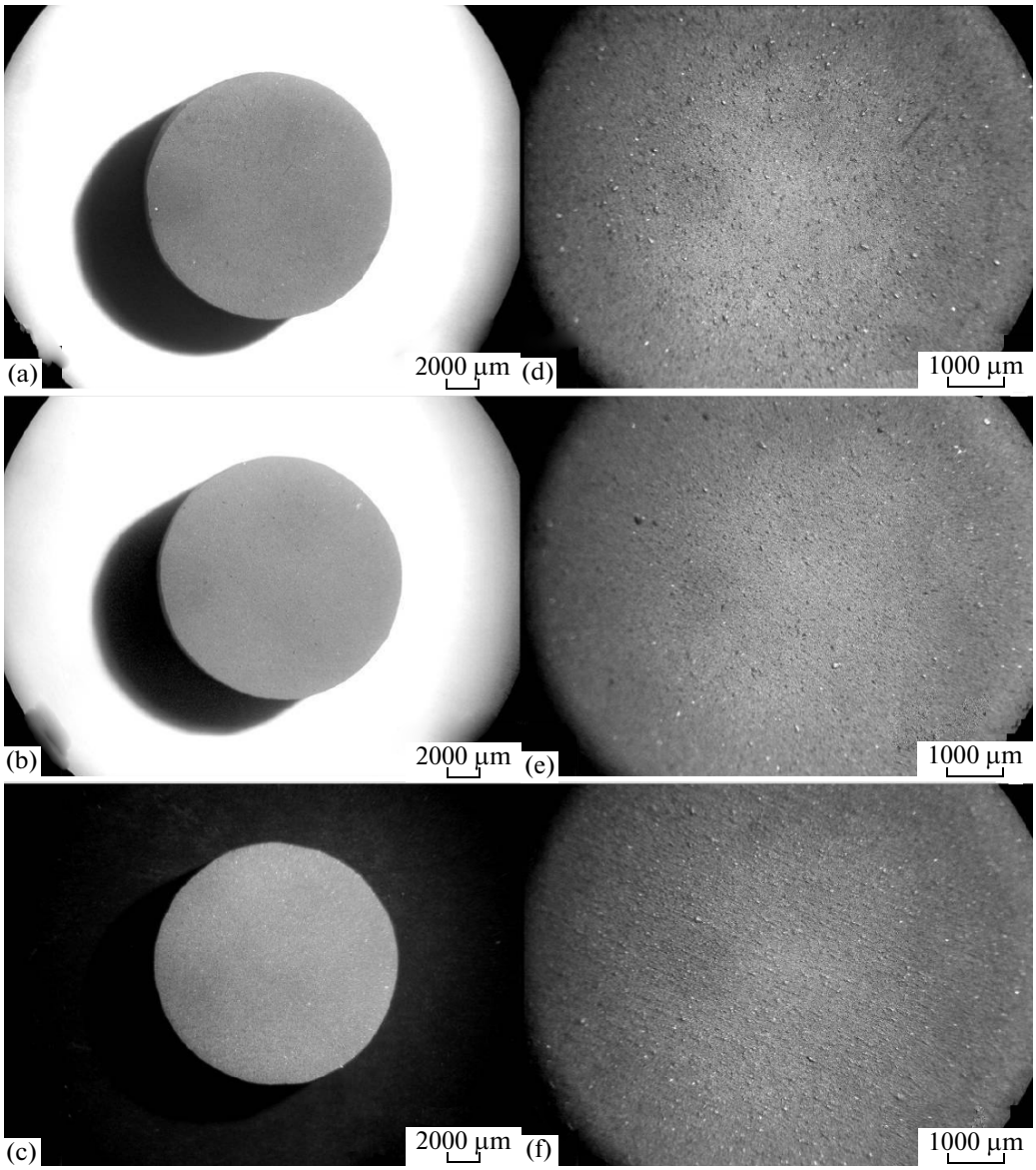

Fig. 1. (a, b, c) External appearance and (d, e, f) surface microstructure of HfB_2-SiC ceramic samples as probed by optical microscopy. SiC percentage, vol %: (a, d) 10, (b, e) 15, and (c, f) 20.

tematically as the silicon carbide percentage increased (sets 2 and 3; see Table 1).

The external appearance of the samples was alike: they were gray cylinders having small prominencies (~20–60 μm in diameter) on their surfaces. Surface microstructure was studied by optical and scanning electron microscopy (Figs. 1, 2). As probed by SEM (Fig. 2), the surface (which consists, in all samples, mainly of well-defined particles with sizes of 2–6 μm) has inclusions of various phase compositions composed of finer particles. As the SiC percentage in ceramic samples increases, the number of these inclusions (which are likely to consist mainly of silicon carbide) increases, too. One can see from micrographs that the samples are rather porous.

The IR transmission spectra for all manufactured samples (as the spectra of the precursor SiC powder, too) feature, along with the absorption band ν(Si–C) at 800–850 cm^{-1}, a low-intensity broad absorption band with a peak at 1070–1080 cm^{-1} associated with the stretching vibrations ν(Si–O) of minor silicon oxide impurity on the surface of SiC particles.

The X-ray diffraction patterns of products feature reflections from a hafnium diboride phase; low-intensity broad reflections from silicon carbide are hardly noticeable on the background, but their intensities increase in response to increasing SiC percentage.

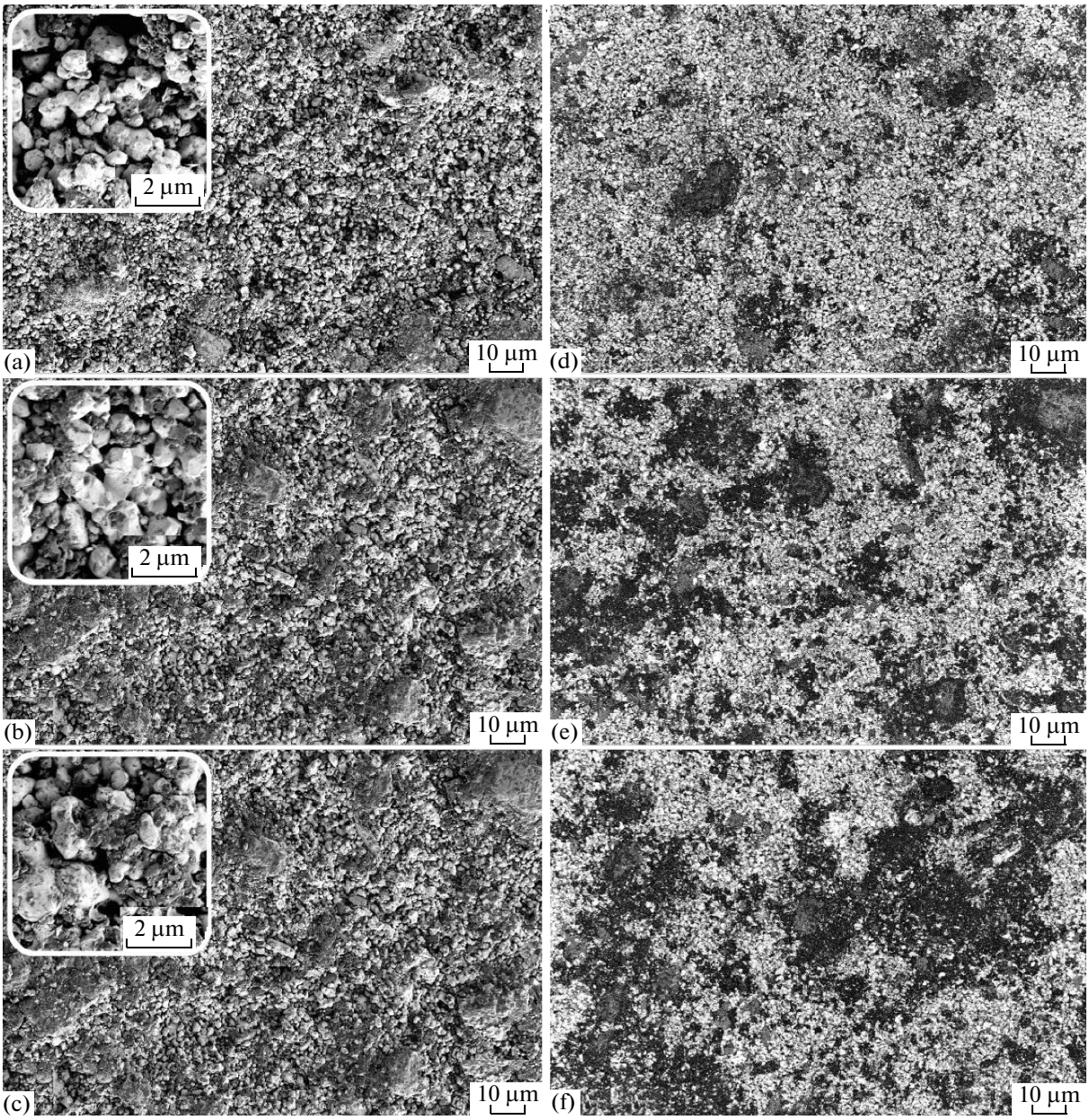

Fig. 2. Surface microstructure of HfB_2-SiC ceramic samples as probed by scanning electron microscopy. SiC percentage, vol %: (a, d) 10, (b, e) 15, and (c, f) 20; (d, e, f) in the phase contrast mode.

Behavior of HfB_2-SiC (10, 15, and 20 vol %) Composite Materials under Heating with a Dissociated Air Stream

To study the behavior of the manufactured HfB_2-SiC ceramic composites under heating by a subsonic stream of dissociated air using a VGU-4 induction plasmatron, a test sample was placed into a water-cooled copper model whose shape was identical to the ESA standard model (which is a flat-end cylinder with a diameter of 50 mm and a rounding edge radius of 11.5 mm). The test sample was mounted at the critical point of the water-cooled copper model by means of bundles of SiC whiskers so that to keep the sample from contact with the model. In order to reduce heat dissipation to the model, the sample was mounted with a 1.5-mm protrusion from the front surface, except for sample 10V-1, whose surface was flush with the holder surface. All experiments employed a subsonic nozzle with an exit cross-sectional diameter of 30 mm; the distance from the nozzle to the sample was also 30 mm, and the initial pressure in the high-pressure chamber of the plasmatron was set at a level of 100 hPa. The parameters of these experiments and surface temperatures are compiled in Table 2.

Table 2. Results obtained from studies of the behavior of samples under exposure to subsonic dissociated air streams of a VGU-4 high-frequency induction plasmatron

Sample no.	Pressure, hPa	Anodic supply power of the plasmatron, kW	Maximal surface temperature*, °C	Overall time of experiment, min	Exposure time at temperatures above 2 000°C*, min	Weight change, %
			Set 1 (10 vol % SiC)			
10V-1[1]	110→120→130→140→150→160→170→200	45→53→64	2670	37	19	+1.0
10V-2	110→120→130→140→150→160**→150	45→53→64	2720	40	32	+0.15
			Set 2 (15 vol % SiC)			
15V-1	110→120→130→140	45→53→64	2740	42	34	–2.0
15V-2	110→170	64→72→64	2740	40	38	–0.1
			Set 3 (20 vol % SiC)			
20V-1	110→120Æ150**→130	45→53→64	2600	35	33	–3.4
20V-2	110→120→130→170**→130	45→53→64	2540, 2600**	40	36	–3.6

[1] The sample is mounted flush with the holder and, at the first step at a temperature of ~1500°C, experienced an extreme cooling with a water stream which gave rise to a crack in the central portion of the sample, but during the second launch of the plasmatron without disassembling the system successfully withstood for more than 36 min without further cracking.

* The temperature as read from a Mikron M-770S pyrometer.

** For a short time.

Sample 10V-1 of set 1. The schedule of exposure of this sample to a dissociated air stream differed appreciably from that employed for the other samples: at the first step, to the sample which was preheated to ~1500°C and mounted flush with the surface, cold water was admitted because of the failure of the cooling system of the holder, after which cooling was stopped. The sample acquired a crack on its surface as a result, but was nonetheless forwarded to the second step of plasma chemical exposure. The variation of the surface temperature of the test sample measured with an M-770S Mikron pyrometer (the value averaged over the surface area of ~5 mm in diameter) is shown in Fig. 3. One can see that the mean surface temperature increases slightly (by 50–100°C) as a result of a stepwise increase in anodic supply power of the plasmatron at a fixed chamber pressure (100 hPa), as well as a subsequent increase in pressure. As probed by a Tandem VS-415U thermal imager (Fig. 4a), the surface was heated comparatively uniformly at the first steps. By the end of the 18th minute under a pressure of 200 hPa, a local overheated region having a temperature of 1900–1950°C appeared at the edge of the sample (Fig. 4b); this region was progressively heated to ~2700°C and grew in size, and this was responsible for a systematic increase in mean temperature (Fig. 3). Noteworthy, the hottest region has not expanded in 37 min so that to occupy the entire surface area of the sample: Fig. 4c displays the thermal image of the surface taken 1 s before the heating was switched off, and so the temperature variation curve in Fig. 3 does not attain a plateau.

Figure 4d shows the external appearance of sample 10V-1 which was withdrawn from the holder after long-term exposure to a dissociated air stream; one can recognize some surface regions that experienced either extremely high temperatures (2600–2700°C), or relatively low temperatures (~1650–1800°C). In addition, a crack caused by abrupt water cooling at the

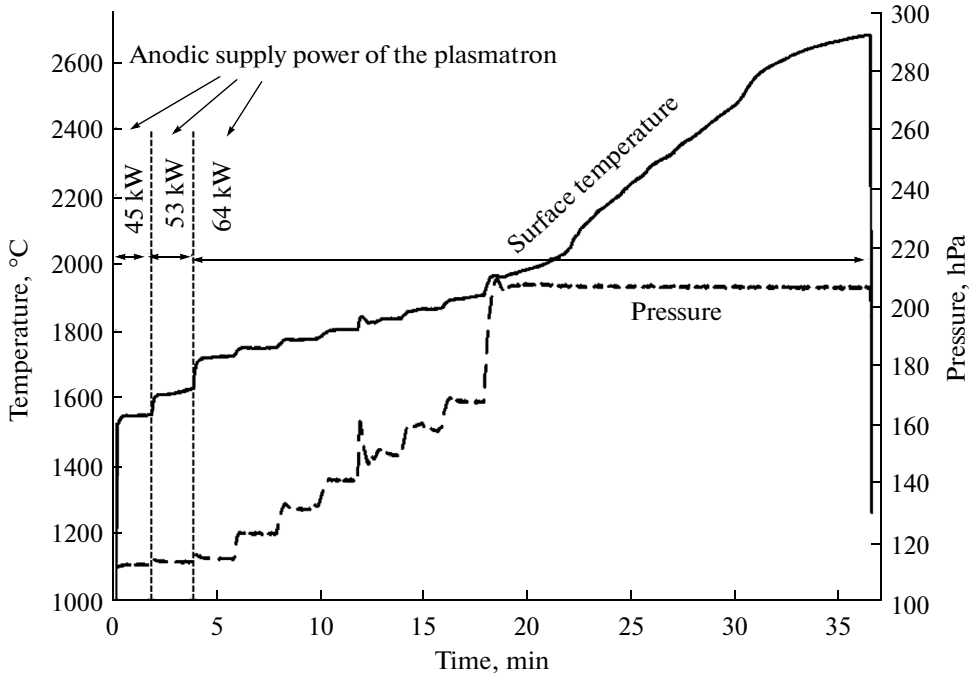

Fig. 3. Surface temperature of sample 10V-1, averaged over the central region ~5 mm in diameter (as measured with a Mikron M-770S pyrometer), chamber pressure, and anodic supply power in the plasmatron during exposure to dissociated air flows (reheating).

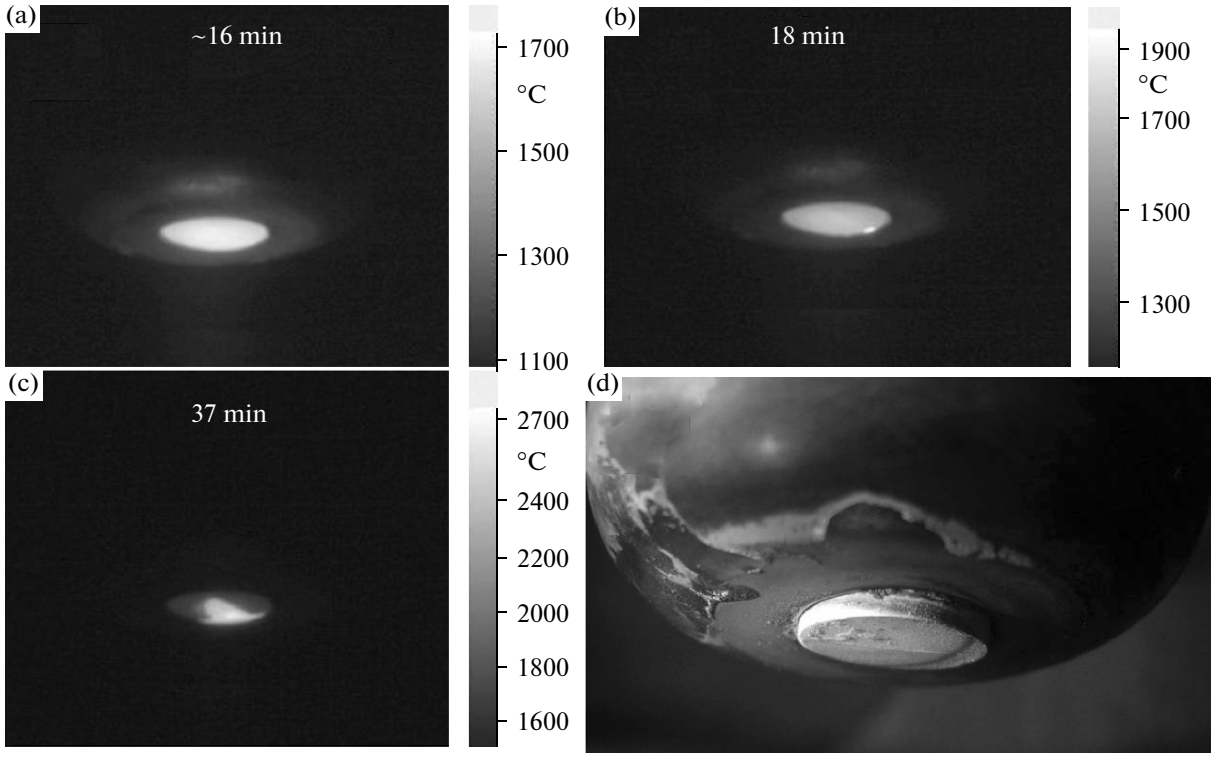

Fig. 4. (a–c) Thermal images of the surface of sample 10V-1 taken in different time periods of the tests and (d) the external appearance of the sample after plasma chemical exposure.

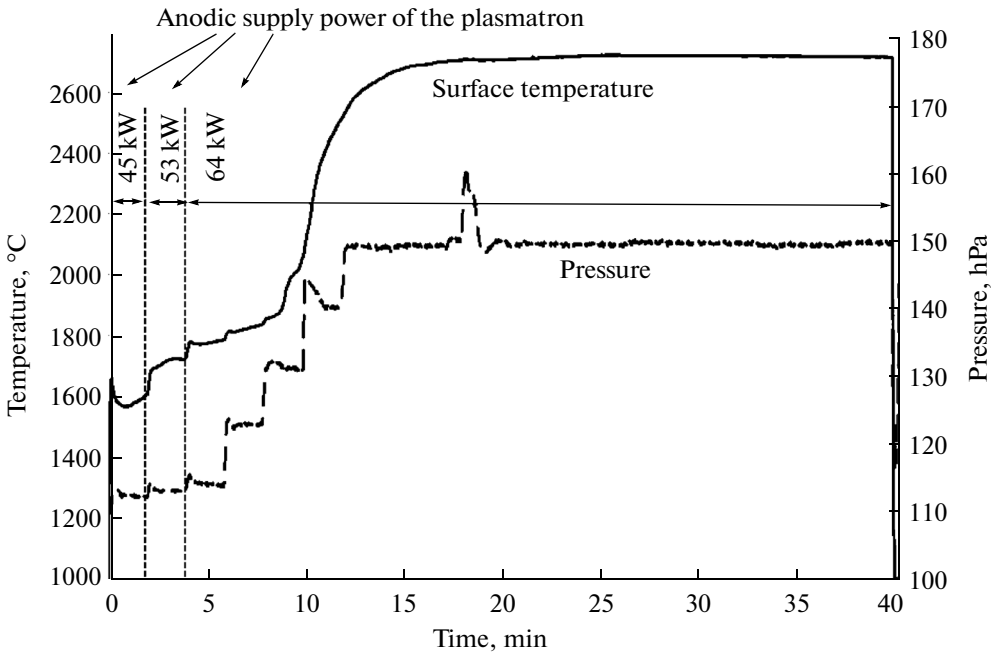

Fig. 5. Surface temperature of sample 10V-2, averaged over the central region ~5 mm in diameter (as measured with a Mikron M-770S pyrometer), chamber pressure, and anodic supply power in the plasmatron during exposure to dissociated air flows.

first step is clearly seen. The weight gain of the sample was 1.0%.

In general, we have to mention that temperature variation in the course of the experiment caused by changing parameters was less noticeable than usual, which can be due to some heat removal as a result of interaction with the water-cooled holder where the sample was mounted flush with the surface of the model.

Sample 10V-2 of set 1. Sample 10V-2, unlike sample 10V-1 of the same composition, was mounted in the holder so that it protruded from the holder by 1.5 mm, and so it had an appreciably different surface temperature variation depending on parameters, namely on the anode supply power and pressure in the high-pressure chamber of the plasmatron (Fig. 5). The temperature variation curve features a temperature peak (which is nonexistent in pre-oxidized sample 10V-1); this peak is probably associated with heat evolution in surface oxidation reactions and is leveled out by the end of the 1st minute of exposure. The mean temperature experiences an insignificant increment as the power and pressure increase; with the maximal power and a pressure of 120 hPa, it begins to rise systematically while only weakly responding to a subsequent increase in pressure. On the 8th minute, the mean surface temperature exceeded 2000°C, and on the 15th minute it was stabilized at a value of 2690–2720°C; as a result, sample 10V-2 was exposed to a dissociated air flow at a mean temperature of less than 2000°C for 32 min, of which 25 minutes were at a surface temperature of ~2700°C.

Thermal imaging gives an explanation to the temperature rise onset on the 8th minute: one can see from Fig. 6b that a progressively expanding crack appears at the edge of the sample with a temperature higher than 2000°C (on the 9th minute, higher than 2600°C). An enlargement of the surface area of this region to occupy the entire surface of sample 10V-2 at the end of the 15th minute (Fig. 6), is responsible for the increase of the mean temperature detected by the pyrometer (Fig. 5).

The transient increase in pressure in the high-pressure chamber of the plasmatron from 150 to 160 GPa in no way influenced the surface temperature, which may serve as indirect evidence that the surface was strongly catalytic.

Figure 6d shows that the surface of sample 10V-2 after testing had a uniform white color of oxidation products of HfB_2-SiC composite. The weight gain of the sample after 40 min of exposure was 0.15%.

Sample 15V-1 of set 2. This sample was subjected to the longest exposure: the overall exposure time was 42 min (Fig. 7).

We must mention that the temperature schedule of sample 15V-1 at the initial stage resembles that for sample 10V-2: an insignificant increase in surface temperature occurred with a stepwise rise in anodic supply power of the plasmatron. The mean temperature started to increase on the 5th–6th minute, which was due to the appearance and enlargement of local overheated areas whose temperature far exceeded 1900–2000°C (Fig. 8a). This processes become most active starting at the 7th–8th minute after the pressure

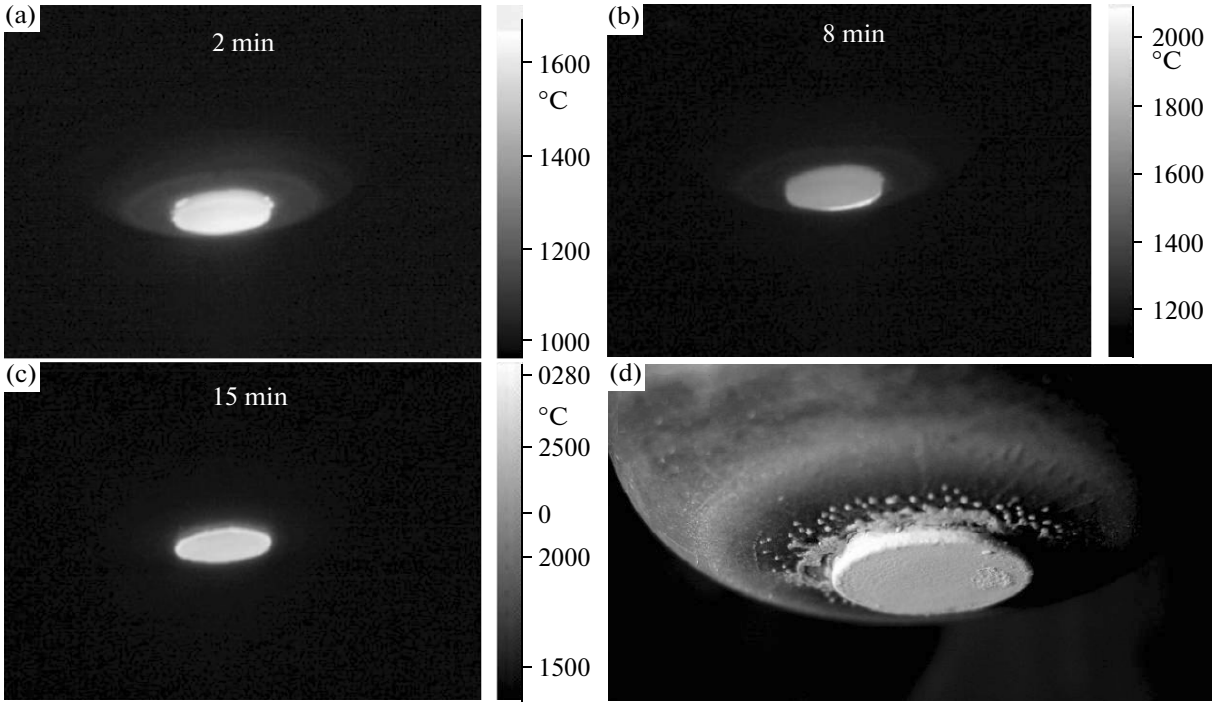

Fig. 6. (a–c) Thermal images of the surface of sample 10V-2 taken in different time periods of the tests and (d) the external appearance of the sample after plasma chemical exposure.

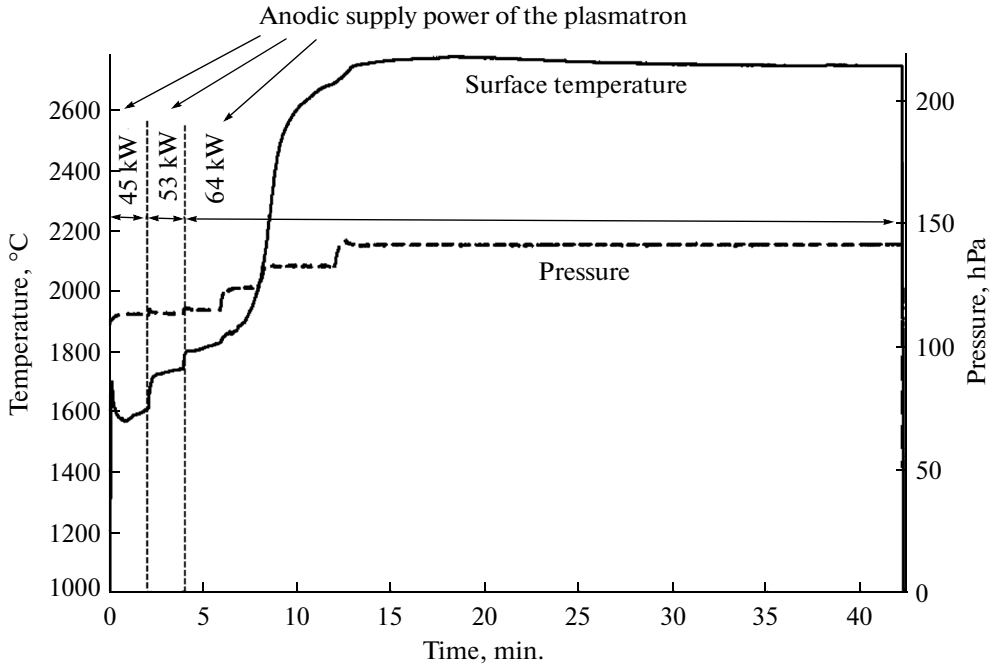

Fig. 7. Surface temperature of sample 15V-1, averaged over the central region ~5 mm in diameter (as measured with a Mikron M-770S pyrometer), chamber pressure, and anodic supply power in the plasmatron during exposure to dissociated air flows.

in the high-pressure chamber of the plasmatron increased from 110 to 120 hPa (Fig. 8b); at the end of the 13th minute, the surface temperature of the sample equalized over all areas at ~2640–2740°C (Fig. 8c). The highest pressure in the high-pressure chamber of the plasmatron in this case was 140 hPa (Figs. 8d, 8e).

After sharp cooling as a result of switched-off heating, the surface temperature of sample 15V-1 lowered

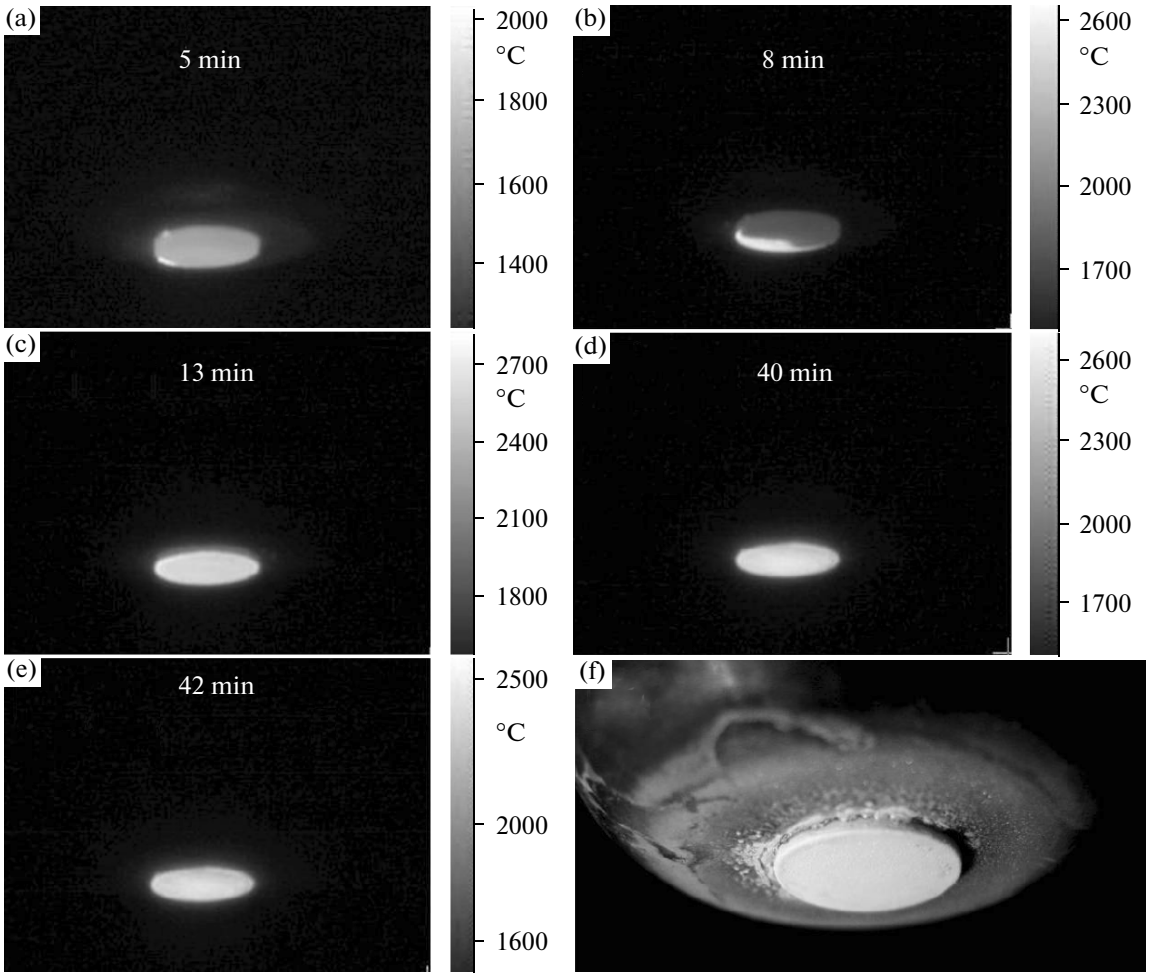

Fig. 8. (a–e) Thermal images of the surface of sample 15V-1 taken in different time periods of the tests and (f) the external appearance of the sample after plasma chemical exposure.

from ~2640–2740 to 1050–1100°C in 5 s, which did not bring about the disintegration or bundling of the sample. The external appearance of sample 15V-1 in the holder after exposure to a dissociated air stream for 42 min is shown in Fig. 8a. The weight loss of the sample was 2.0%, which may be associated with intense evaporation of boron- and silicon-containing products from the surface at extremely high temperatures (2600–2740°C) and relatively low pressures in the high-pressure chamber of the plasmatron.

Sample 15V-2 of set 2. The plasma chemical experiment involving sample 15V-2 was purposed to study its behavior under rapid heating to high temperatures. For this purpose, the sample was introduced into a dissociated air stream with the 64-kW anodic supply power of the plasmatron, which was the maximal value for all of the experiments described here; the pressure in the chamber also increased from 100 to ~167–170 hPa in 1.5–2 min.

The surface temperature variation of the sample is shown in Fig. 9. One can see that the surface temperature at the 2nd–3rd minute exceeded 2000°C as a result of the rapid expansion of a local overheated area (having a temperature of ~2700°C) that emerged on the periphery of the sample whose temperature was 1700–1800°C (Figs. 10a–10c). Thus, in 11 minutes the surface temperature was at a level of 2700–2710°C. The transient (from 13th through 14 minute) increase in the anodic supply power of the plasmatron to 72 kW gave rise to a ruse in temperature to 2740–2750°C, and after the 64-kW power was recovered, the temperature returned to the previous level of ~2700°C. On the 15th minute, one can trace, in the thermal image, the appearance of a region with a slightly lower (by ~100°C) temperature, which survived to the end of the experiment. The external appearance of the sample in the holder after tests is shown in Fig. 10d. The overall weight loss of the sample in 40 min of exposure to a dissociated air stream was 0.1%.

Sample 20V-1 of set 3. Exposure of this sample to dissociated air streams was also controlled through changing the anodic supply power of the plasmatron

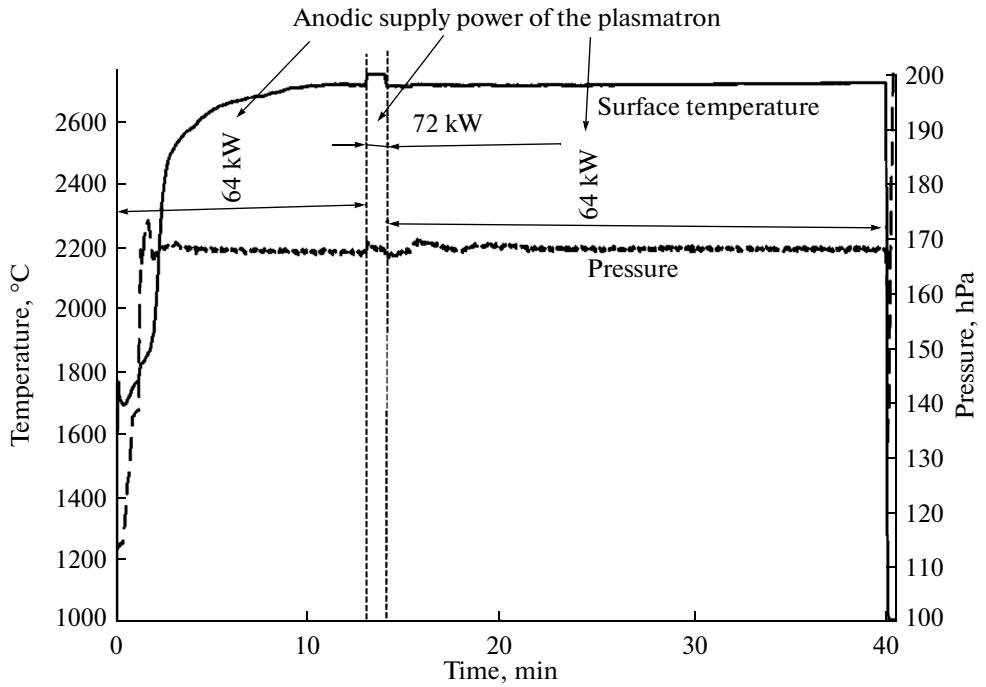

Fig. 9. Surface temperature of sample 15V-2, averaged over the central region ~5 mm in diameter (as measured with a Mikron M-770S pyrometer), chamber pressure, and anodic supply power in the plasmatron during exposure to dissociated air flows.

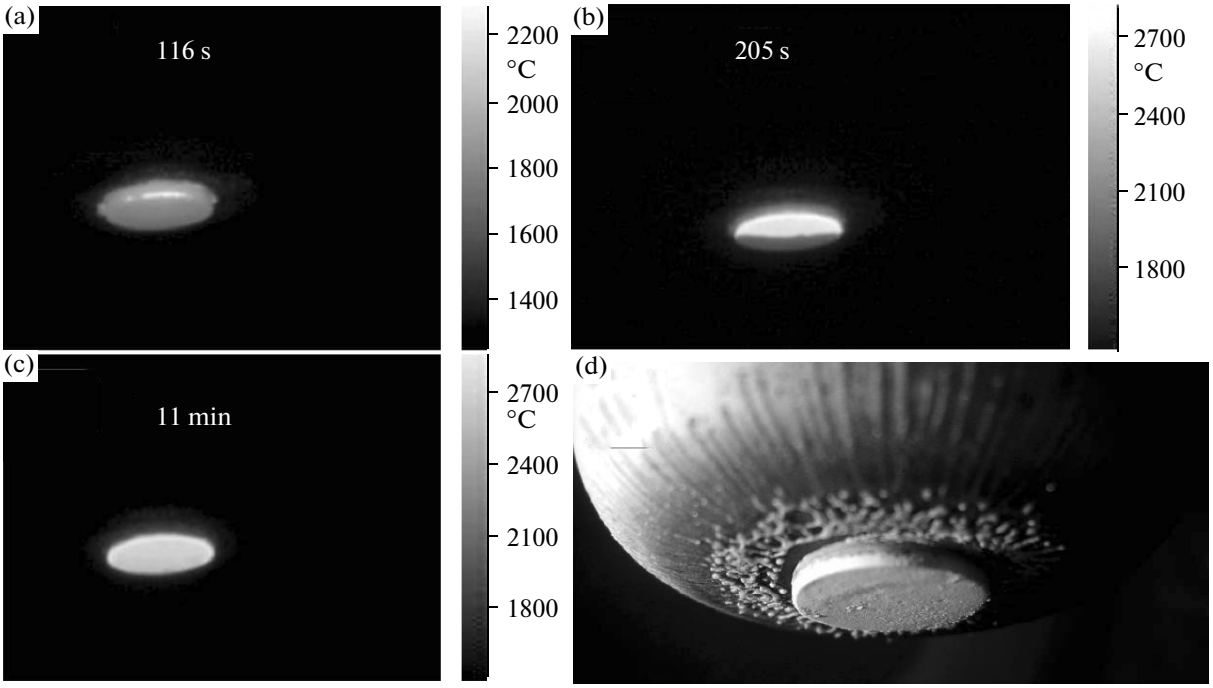

Fig. 10. (a–c) Thermal images of the surface of sample 15V-2 taken in different time periods of the tests and (d) the external appearance of the sample after plasma chemical exposure.

from 45 to 53 and then to 64, followed by stepwise increasing pressure in the chamber (Fig. 11). One can see that the surface temperature increases as early as at the first stage of the experiment with minimal power and pressure values to exceed 2000°C in the beginning of the 3rd minute (Fig. 12a), and this strongly distinguish the behavior of this sample from the behavior of samples of sets 1 and 2. At the end of the 2nd minute,

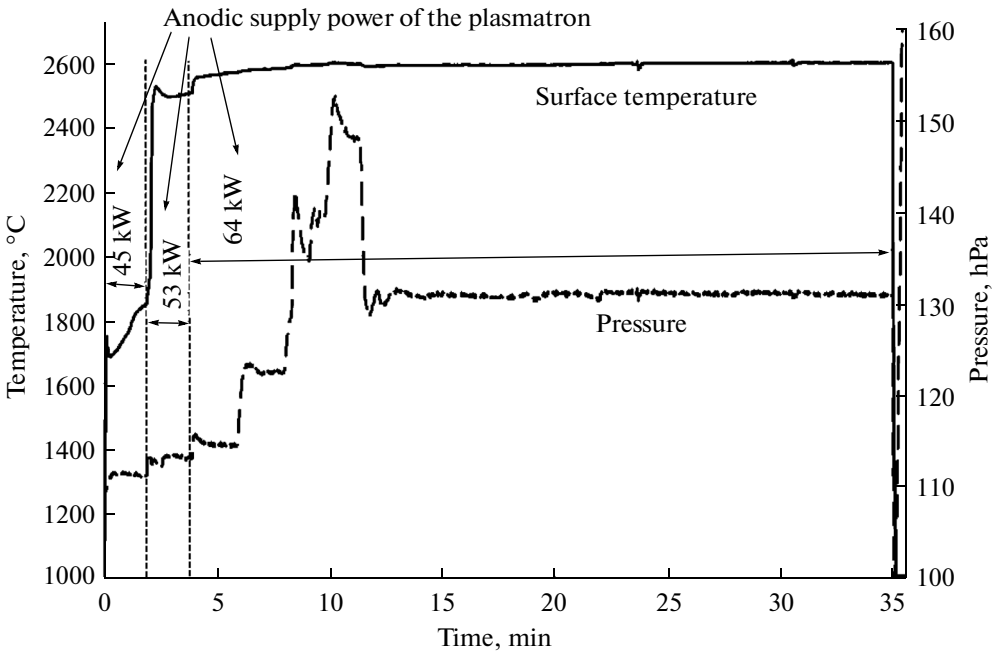

Fig. 11. Surface temperature of sample 20V-1, averaged over the central region ~5 mm in diameter (as measured with a Mikron M-770S pyrometer), chamber pressure, and anodic supply power in the plasmatron during exposure to dissociated air flows.

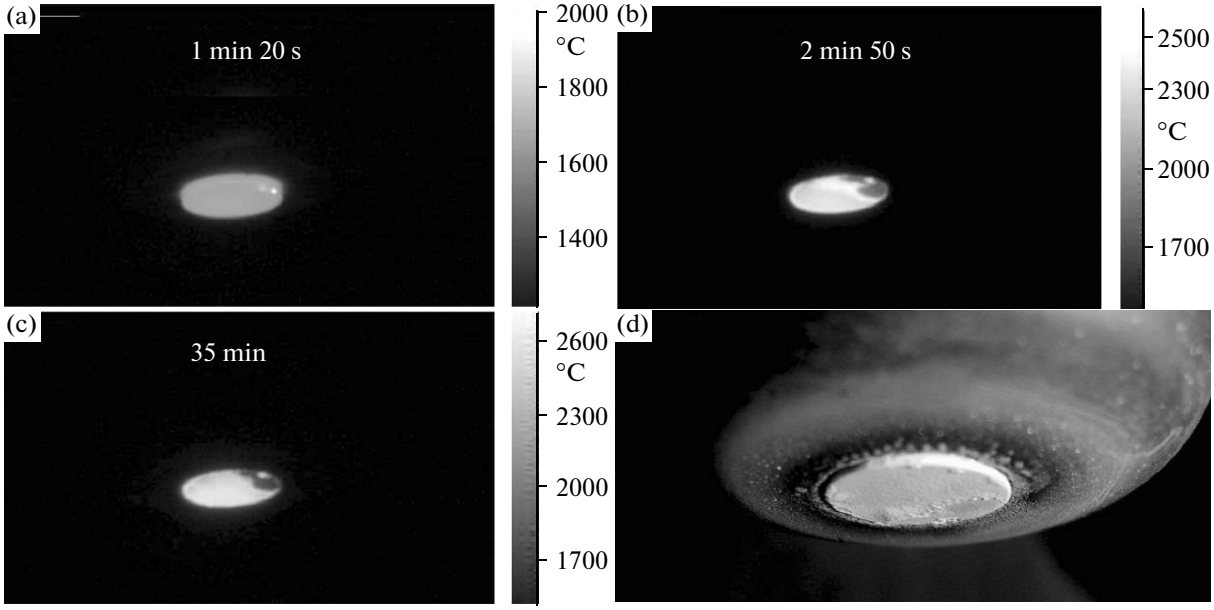

Fig. 12. (a–c) Thermal images of the surface of sample 20V-1 taken in different time periods of the tests and (d) the external appearance of the sample after plasma chemical exposure.

the sample was pushed by the gas flow into the holder (the protrusion size was ~0.5 mm as a result), then the surface temperature acquired a value of 2370–2440°C with a rise to 2550–2610°C, except for small areas that had lower temperatures (1800–1900°C), which were reduced in size only insignificantly as the power and pressure increased further (Figs. 12b, 12c).

We must mention that when the anodic supply power of the plasmatron increased from 53 to 64 kW, the mean temperature increased little (by ~50°C), and an appreciable increase in pressure from 120 to 153 hPa had almost no effect on the surface temperature of sample 20V-1 (the rise was ~15°C), which may indicate the high surface catalyticity in surface recombina-

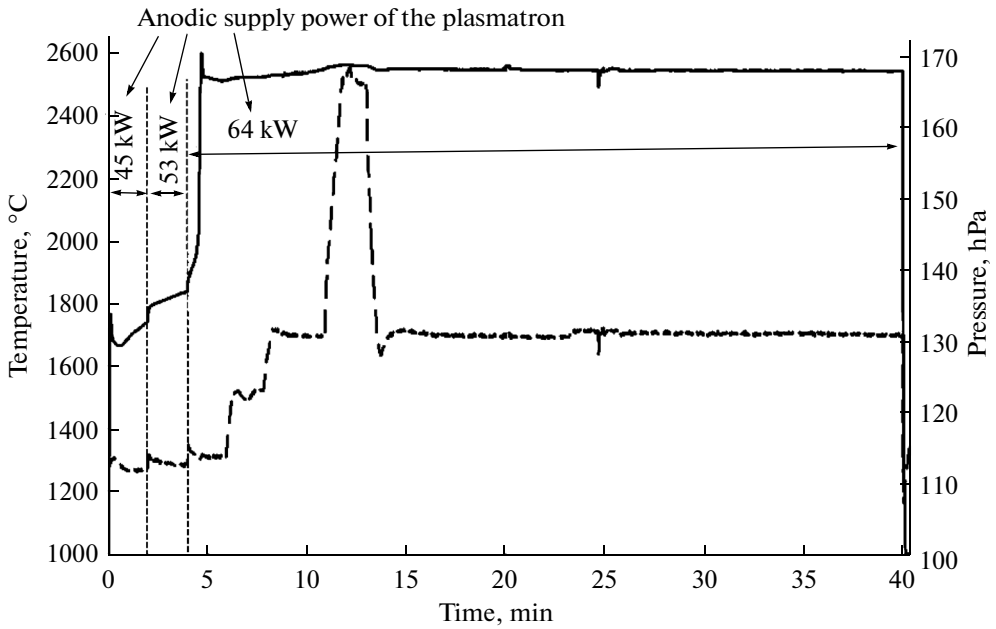

Fig. 13. Surface temperature of sample 20V-2, averaged over the central region ~5 mm in diameter (as measured with a Mikron M-770S pyrometer), chamber pressure, and anodic supply power in the plasmatron during exposure to dissociated air flows.

tion of oxygen and nitrogen atoms. The external appearance of the sample in the holder after tests is shown in Fig. 12d: the larger surface area which corresponds to the high-temperature test is white in color, while low-temperature areas have a gray tint (thermal images and micrographs were taken from opposite sides of the unit). The weight loss 35 min of exposure to a dissociated air stream was 3.4%.

Sample 20V-2 of set 3. The exposure protocol for this sample repeats that for compositionally similar sample 20V-1 (Fig. 13). The difference consists in that sample 20V-2 was partially pushed into the holder by the gas flow as early as at the initial stage, resulting in an inclination of the front surface and thereby improving heat dissipation and slowing down the full heating of the surface of the sample. Thus, the attainment of temperatures higher than 2000°C and the onset of an active rise in temperature occurred at the third heating stage when the anodic supply power of the plasmatron was 64 kW and the pressure had a minimal value of 110 hPa (Fig. 14b), although a slow increase in mean temperature of the sample was observed as early as at the first stage.

One can see that the surface temperature of the sample was 2530–2550°C most of time (for more than 35 min), and an appreciable increase in pressure to ~170 hPa almost did not change this value (the rise was ~15°C). The weight loss of the sample was 3.6%.

Characterization of HfB_2-SiC (10, 15 and 20 vol % SiC) Samples after Exposure to Dissociated Air Streams

Surface roughness was measured in all samples after plasma chemical exposure. Different regions of sample 10V-1, where temperatures were appreciably different during the experiment were found to have different roughnesses. In a hot area which experienced temperatures of 2600–2700°C, the roughness was reduced: R_a was 1.1 μm, i.e., more than twice lower than for the intact sample. In the areas where the temperatures were ~1650–1800°C, R_a values were ~3.0 μm. For sample 10V-2 whose surface temperature exceeded 2600°C during the tests, the parameter R_a increased twice to become also 3.0 μm. For samples of set 2, the parameter R_a also increased twofold to become 3.2 (in sample 15V-1) and 4.7 μm (in sample 15V-2). In sample 20V-1, both the hot and the cold areas experienced an increase in R_a (to 3.4 and 2.9 μm, respectively), while in sample 20V-2 (which has the same composition and exposure protocol), the mean roughness remained almost unchanged: R_a ~1.5 μm.

The X-ray powder diffraction patterns recorded from the front surface showed that monoclinic HfO_2 was the only crystalline phase identified in all samples except for sample 10V-1 (Fig. 15).

For sample 10V-1, additional reflections corresponding to hafnium silicate $HfSiO_4$ phase are observed. Likely, from the data earlier obtained for a sample having an appreciably higher SiC percentage SiC (45 vol %) [7], one can infer that the formation of this phase is typical in case of high pressures (200 hPa) and when the surface temperature during the plasma chemical experiment is lower than 1800–1900°C in the cold areas formed for sample 10V-1.

This inference is indirectly supported by the absence of reflections from the $HfSiO_4$ phase in the X-ray diffraction pattern of compositionally similar sample 10V-2, whose surface was uniformly heated to

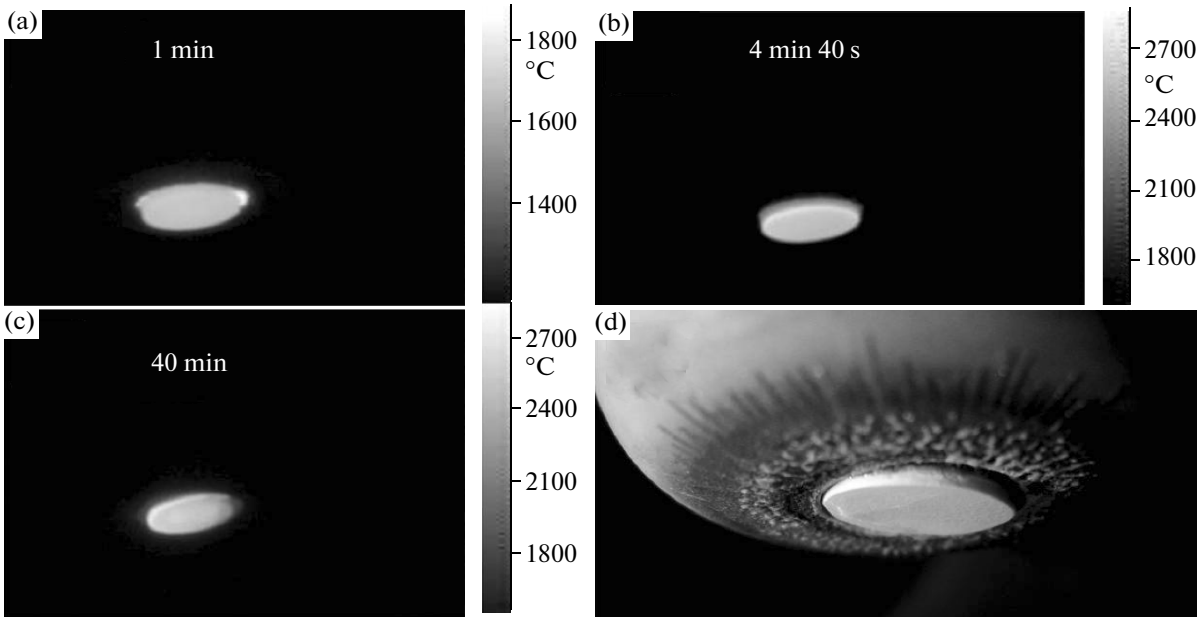

Fig. 14. (a–c) Thermal images of the surface of sample 20V-2 taken in different time periods of the tests and (d) the external appearance of the sample after plasma chemical exposure.

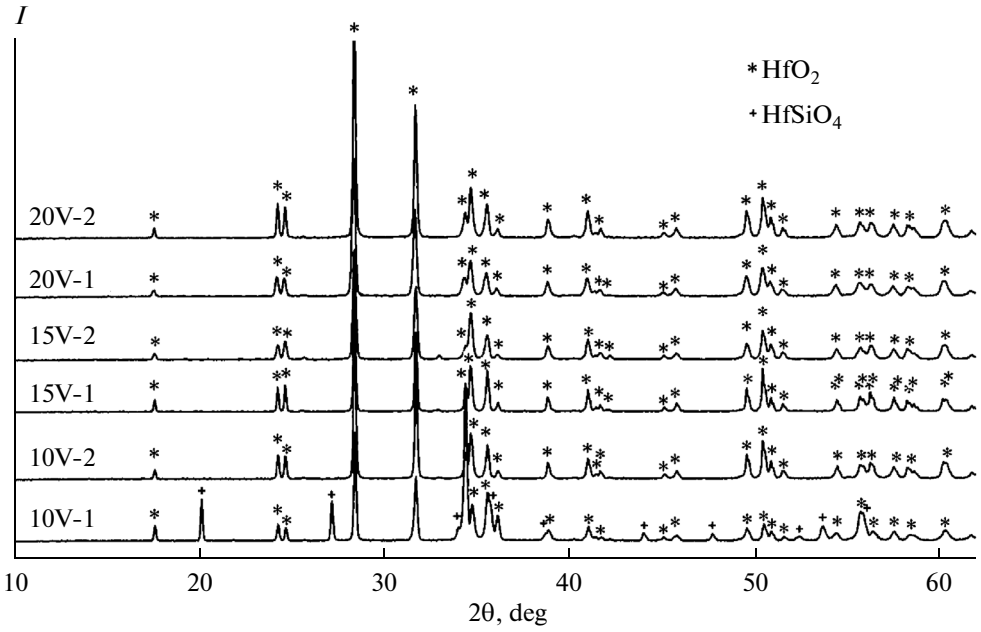

Fig. 15. X-ray diffraction patterns recorded from the front surfaces of HfB_2-SiC (10, 15, and 20 vol % SiC) samples after exposure to dissociated air flows.

2690–2720°C during exposure to a dissociated air stream. Further, the exposure conditions for sample 10V-2 favored removal of boron- and silicon-containing oxidation products: the experiment was carried out at appreciably lower pressures in the high-pressure chamber and longer exposure times at maximal temperatures, which is also proven by the difference in weight change as a result of concurrent oxidation and evaporation of liquid products (components of newly formed borosilicate glass).

For samples of sets 2 and 3, a hafnone phase was absent on the front surface, regardless of whether areas with temperatures lower than 2000°C were observed or no; this may be explained by longer exposure times (at least 33 min) at a mean surface temperature or ~2550–2740°C and at relatively low pressures (≤130–

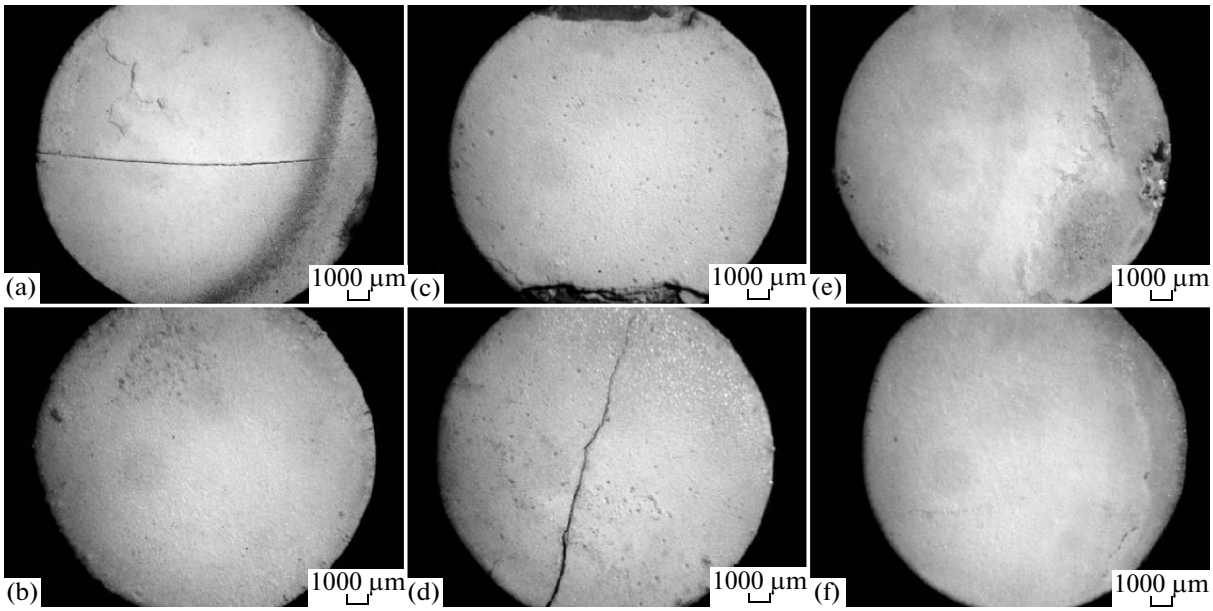

Fig. 16. External appearance of the front surfaces of HfB_2-SiC samples after exposure to dissociated air flows: (a) sample 10V-1, (b) sample 10V-2, (c) 15V-1, (d) 15V-2, (e) sample 20V-1, and (f) sample 20V-2.

140 hPa, with transient increases). Some exception is sample 15V-2; in the experiment with this sample the pressure was 170 hPa, but the nonappearance of the $HfSiO_4$ phase is likely to be due to a longer exposure time (38 min) at a temperature higher than 2000°C.

Figure 16 shows the external appearance of samples after exposure to dissociated air streams. For sample 10V-1, one can clearly see the crack resulting from rapid cooling with water at the first stage of exposure to air plasma; one can also see an area that had a lower temperature (not higher than 1800°C) during the experiment, as distinct from the most surface area of the sample. For the other samples, the oxidized surface has the appearance of white porous ceramics. Exceptions are the samples with the highest silicon carbide percentage (20 vol %), whose surface also has gray areas where temperatures were appreciably lower than over most surface areas of the samples, with a characteristic glassy luster. It is worth noting that the crack observed in sample 15V-2 was not formed in the course of exposure; rather it appeared during storage of the sample in 2 weeks after the test (it is likely that stress relaxation or damage occurred during the removal from the holder).

Scanning electron microscopy was used to gain more details of the surface microstructure of samples after plasmatron experiments (Figs. 17–22).

Very interesting is the situation where the surface of a sample, apart from a greater area exposed to temperatures of 2600–2700°C, has some areas where the temperature during the experiment was relatively low (less than 1800–1900°C). Sample 10V-1 experienced the least high-temperature exposure: the exposure time at a mean temperature above 2000°C for this sample was as short as 19 min; there were opportunities for more active heat exchange with the holder, because the sample was mounted in the holder without protrusion; during half of the total test time, the highest pressure of all the experiments (200 hPa) was maintained in the high-pressure chamber of the plasmatron, and this should intensify oxidation processes and counteract the high-temperature evaporation of the components of borosilicate glass from the surface. As a result one can see that the complete evaporation of boron- and silicon-containing components did not occur even in the central region (Figs. 17a, 17b) where temperatures of 2600–2700°C were observed, and borosilicate glass occurs in the pores of a refractory HfO_2 skeleton at relatively small depths. An entirely different picture was observed on the surface areas where the temperature did not exceed 1800°C (Figs. 17c, 17d): their surfaces are fully covered with the glass extruded from the pores of by excessive pressure of SiO(g) and CO(g) [29–31], the surface of which bears solidified bubbles indicating the occurrence of gas formation or evaporation. Phase contrast data allow us to say that the conditions created on such surface areas kept the HfO_2 skeleton from yielding to the surface (this is also indicated by EDX data: the hafnium percentage is as low as 3.6 at % against the silicon percentage of 18.5 at %). Matching X-ray powder diffraction data with the existing picture, we may assume that the concentration conditions (sufficiently high SiO_2 percentage) and temperature conditions enabled hafnone $HfSiO_4$

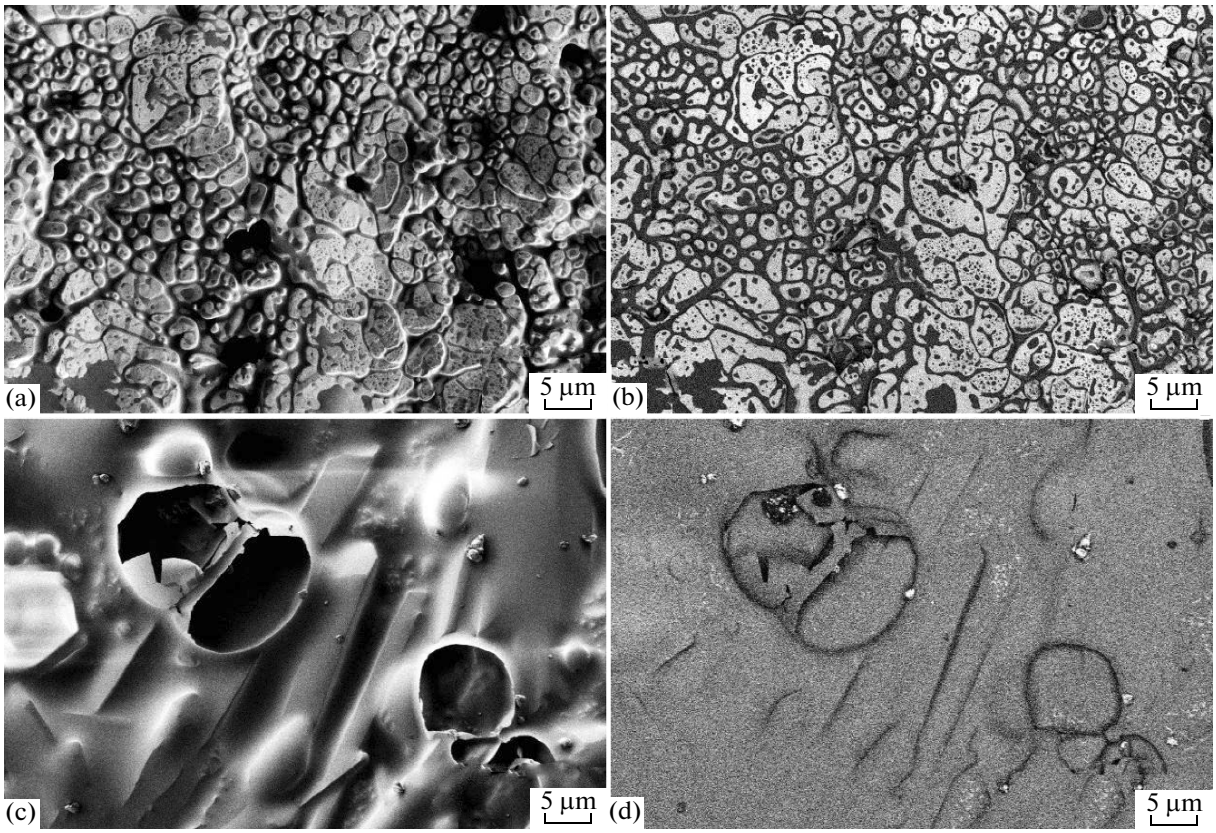

Fig. 17. Surface microstructure of sample 10V-1 of set 1 after exposure to dissociated air flows (as probed by SEM): (a, c) surface morphology as probed by a secondary electron detector for (a) hot area and (c) cold area and (b, d) in the atomic number averaged contrast mode.

to crystallize upon rapid cooling; this is not in contrary to the HfO_2–SiO_2 phase diagram [32].

For compositionally similar sample 10V-2 which also comprises 10 vol % SiC and was subjected to a more severe exposure [longer exposure times (~25 min at 2600–2700°C and 32 min at temperatures higher than 2000°C) and an appreciably lower pressure in the high-pressure chamber of the plasmatron, which should intensify the volatilization of boron and silicon oxides], a porous structure was formed throughout the entire surface area of the sample; this structure consisted mostly of hafnium dioxide (silicon was not detected by EDX on the surface). Probably, the protective borosilicate glass layer was in the deeper lying regions of the multilayer near-surface oxidized region of the sample as a result of active evaporation from the surface.

For sample 15V-1 (Fig. 19), a higher porosity of surface microstructure was observed (there was a high proportion of large pores with sizes of 20–50 μm). Energy-dispersive analysis of the 6-mm^2 central area showed that this area consisted mostly of HfO_2 with an insignificant silicon impurity.

A similar situation is for sample 15V-2, which belongs to the same set 2 and has a very similar surface microstructure (Fig. 20): an incipiently melted porous HfO_2 skeleton was observed and no borosilicate glass was detected on the surface (EDX did not show silicon traces). It is likely that the higher pressure in the high-pressure chamber of the plasmatron compared to that in the experiment on sample 15V-1 (for sample 15V-1, $P \leq 140$ hPa and a transient hypersonic conditions were created) were compensated for at $P = 170$ hPa by a long-term exposure at temperature higher than 2700°C (32 min against 25 min for sample 15V-1).

For both samples of set 3, conditions were created such that areas having temperature below 1850°C were formed on the surface, most area of which was heated to 2500–2600°C. This impacted both the microstructure and chemical composition of these areas. It is pertinent in this regard that the cold areas were also exposed for 34 and 38 min at relatively low pressures in the high-pressure chamber (mostly of 130 hPa), which should have favor the evaporation of more volatile components.

So, sample 20V-1, whose exposure was less long than for its analogue 20V-2, mostly formed the microstructure of a porous ceramic skeleton of HfO_2 (as for the other samples, except for 10V-1), which is verified by elemental analysis (no silicon impurity was

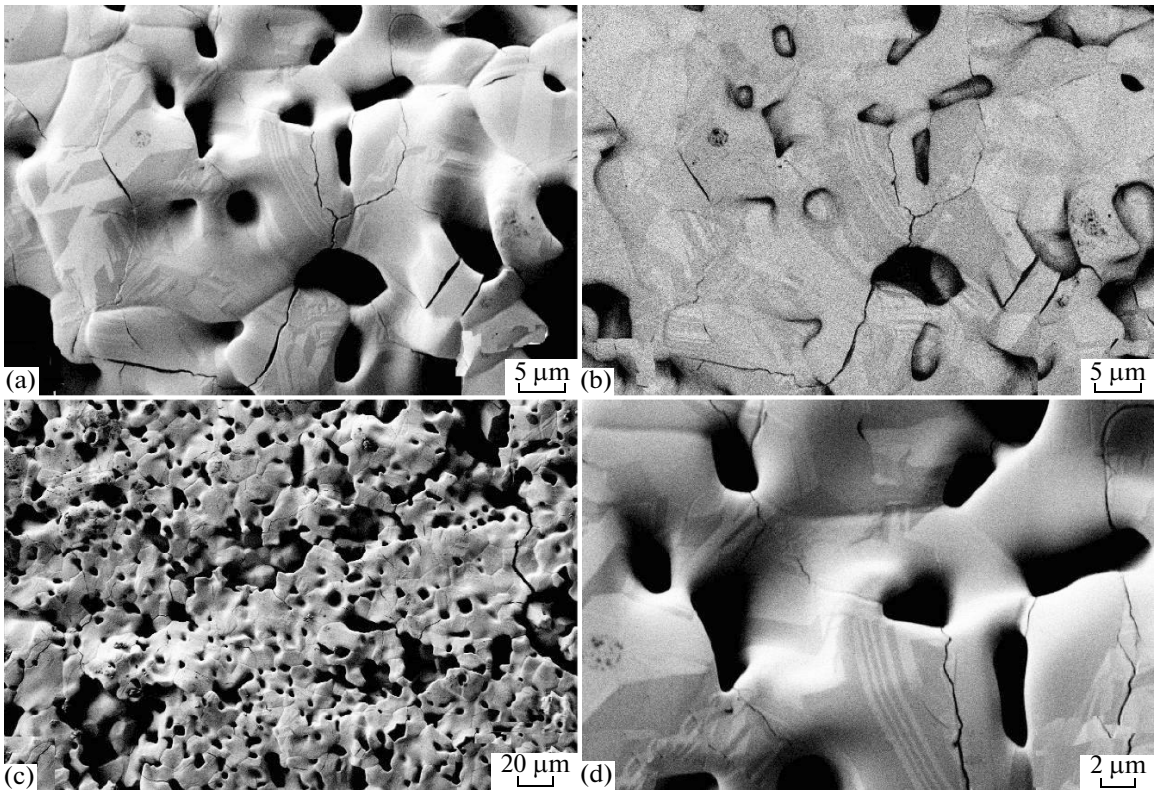

Fig. 18. Surface microstructure of sample 10V-2 of set 1 after exposure to dissociated air flows (as probed by SEM): (a, c, d) surface morphology as probed by a secondary electron and (b) in the atomic number averaged contrast mode.

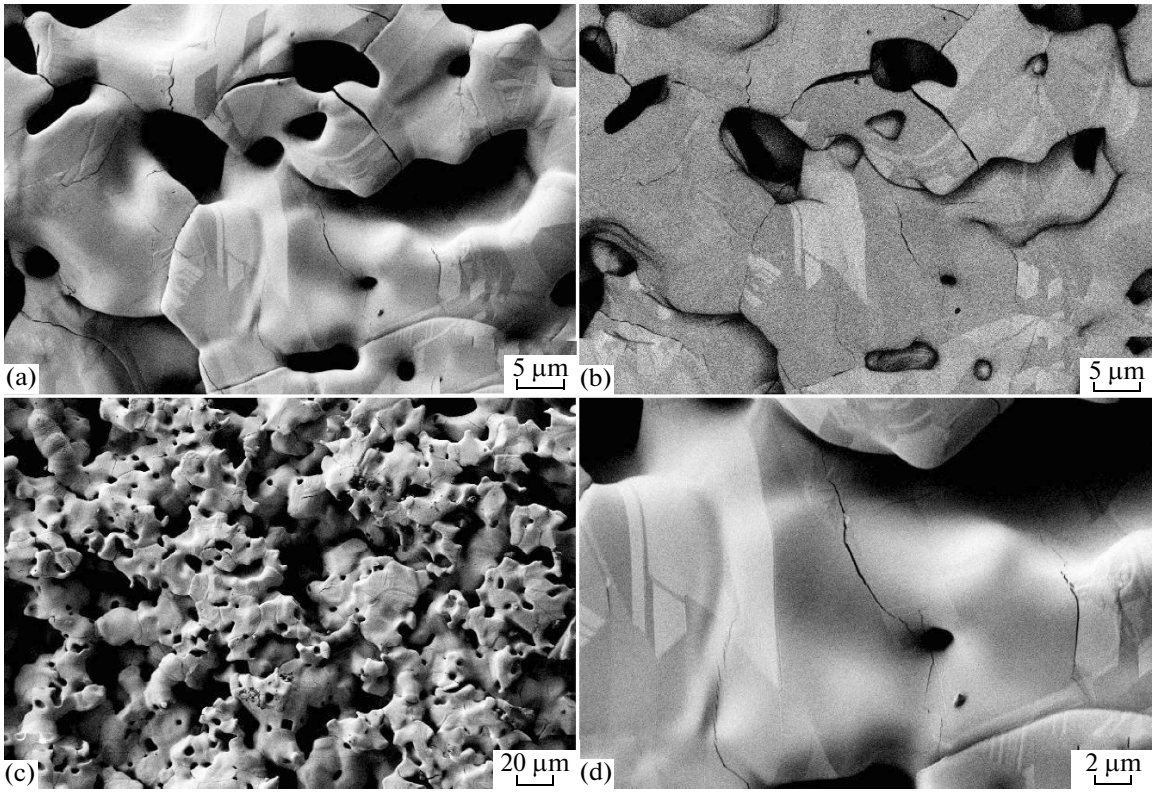

Fig. 19. Surface microstructure of sample 15V-1 of set 2 after exposure to dissociated air flows (as probed by SEM): (a, c, d) surface morphology as probed by a secondary electron and (b) in the atomic number averaged contrast mode.

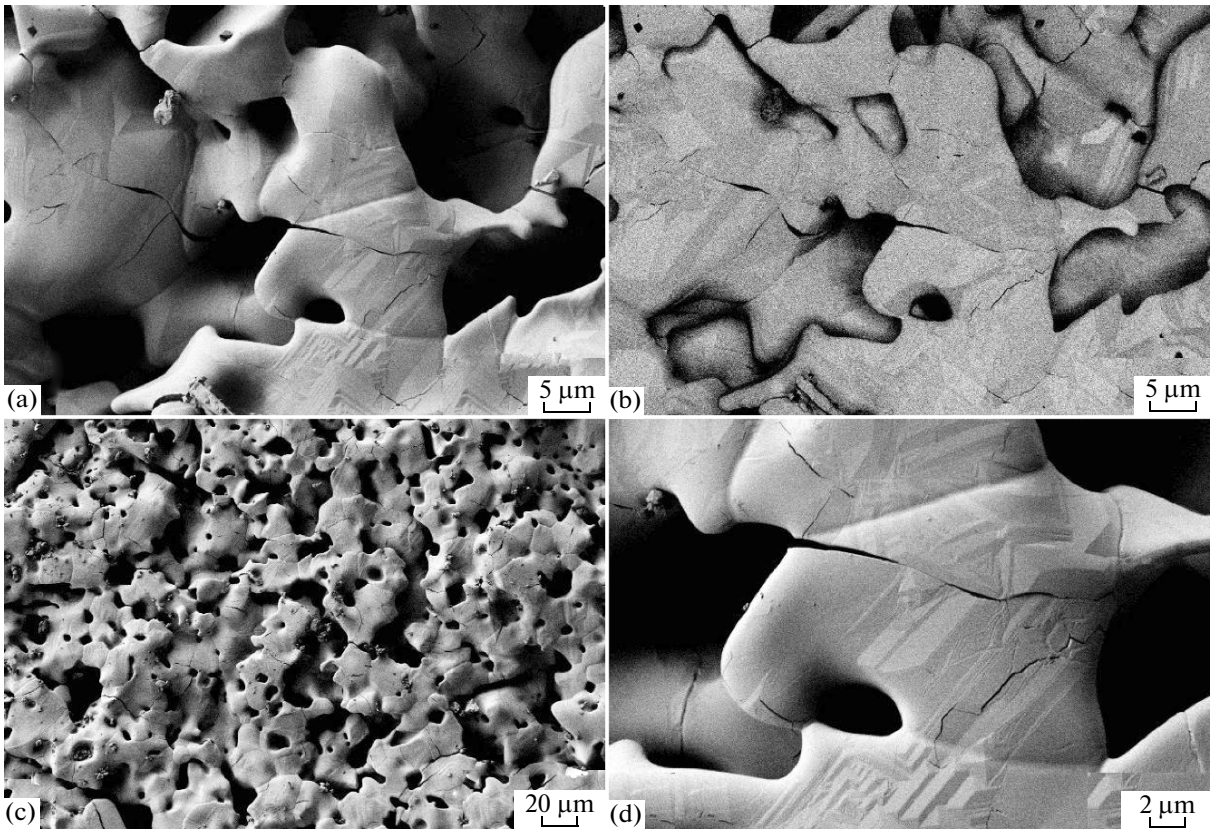

Fig. 20. Surface microstructure of sample 15V-2 of set 2 after exposure to dissociated air flows (as probed by SEM): (a, c, d) surface morphology as probed by a secondary electron and (b) in the atomic number averaged contrast mode.

detected on ~6-mm^2 central surface area). On cold areas (Figs. 21c, 21d), one can see that the surface-yielding HfO_2 skeleton is partially filled with borosilicate glass. Energy-dispersive analysis showed that, despite the absence of silicon-containing crystalline phases, silicon oxide on the surface (Fig. 15) in this area (silicon percentage is ~19 at %) prevails over HfO_2; the latter performs the role of a skeleton (hafnium percentage is ~3–4 at %), which starts to manifest itself over partially evaporated and deeper buried glass.

The surface microstructure of sample 20V-2 may be described in the same manner: a porous hafnium dioxide surface layer dominates (silicon as absent on the surface as probed by EDX analysis), and is accompanied with glass in the areas that were heated to lower temperatures during the plasma chemical experiment (Fig. 22). The following is noteworthy: since this sample experienced a longer exposure to a dissociated air stream, the degree of borosilicate glass evaporation from the surface was higher. Figures 22c and 22d show that, unlike the situation with sample 20V-1, large pores are formed in the HfO_2 skeleton and glass only slightly wets it because of having high wettability on zirconium and hafnium dioxides. Energy-dispersive analysis of these areas showed higher hafnium percentages compared to sample 20V-1 (15–20 at %), but the silicon fraction was also considerable (6–11 at %).

On the whole, we may say that porous ceramic hafnium dioxide skeleton was formed on the surfaces of samples of all sets (containing 10, 15, and 20 vol % SiC), which were heated by dissociated air streams to temperatures of 2550–2700°C. When there were areas with appreciably lower temperatures, the chemical composition and surface microstructure were strongly influenced by specific exposure conditions, primarily the pressure in the high-pressure chamber of the plasmatron (which influences the bulk oxygen concentration and the conditions of possible evaporation of boron and silicon oxides from the surface) and the exposure length and temperature.

The oxidation of HfB_2-SiC materials in the bulk was studied using optical microscopy (Fig. 23) and scanning electron microscopy (Fig. 24). Figure 23 shows, as examples, sectional images of samples 10V-2, 15V-1, and 20V-1 (panel c), which were exposed to dissociated air streams under similar conditions (especially in regard of the variation of anodic supply power of the plasmatron). One can see that a multilayer oxidized area was formed with a thickness ranging from about

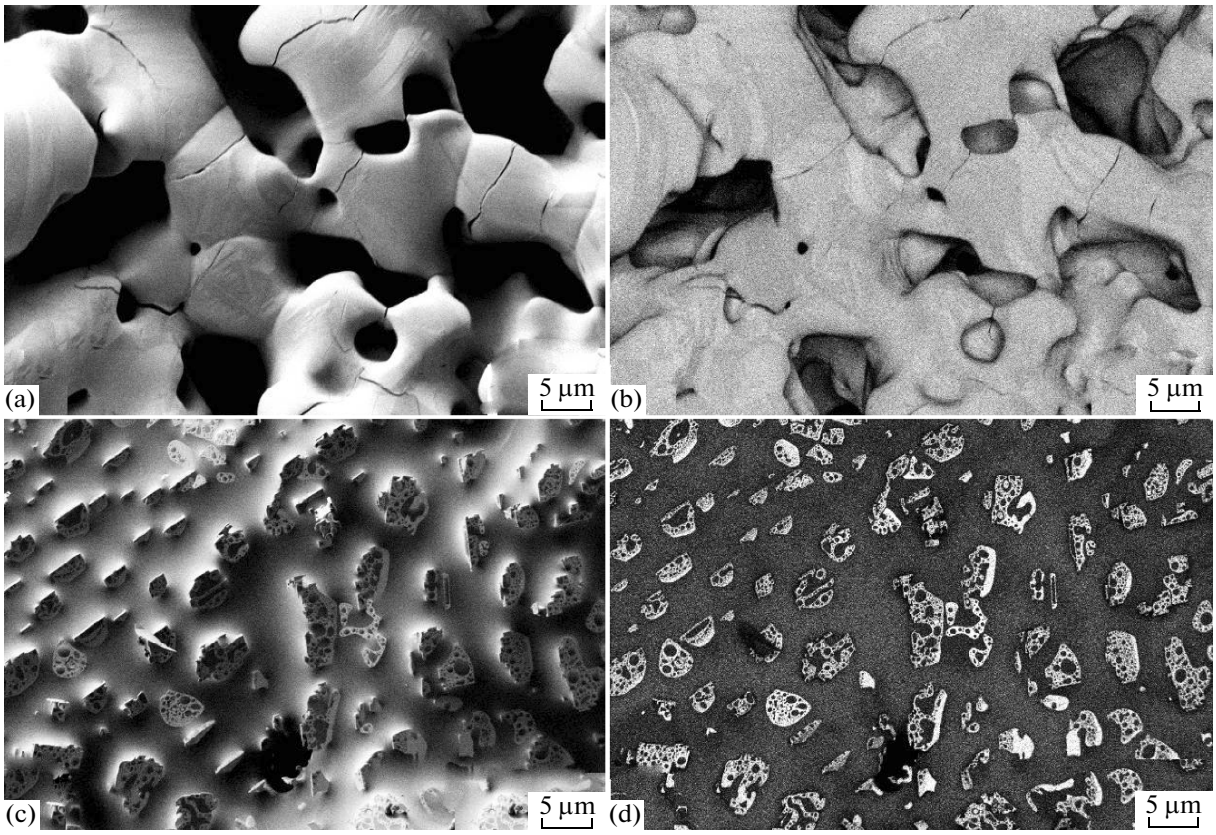

Fig. 21. Surface microstructure of sample 20V-1 of set 3 after exposure to dissociated air flows (as probed by SEM): (a, c) surface morphology as probed by a secondary electron detector for (a) hot area and (c) cold area and (b, d) in the atomic number averaged contrast mode.

100 μm (for areas where the temperature did not exceed 1850–1900°C in the course of plasma chemical exposure; see Fig. 23c, right-hand image) to 800–1000 μm for hot areas where the surface was heated to and exposed for more than 20–30 min at 2550–2700°C. A rather porous surface layer is formed (likely based on refractory HfO_2), underlain by more dense layers where the pores of the HfO_2 skeleton was fully filled with oxygen diffusion protecting borosilicate glass produced by the oxidation of the HfB_2-SiC material. Some samples have glass-filled pores extended along the surface.

SEM data for sections of the same samples (Fig. 24) make it possible to have insight into more details of the microstructure and to estimate the elemental composition of each layer. The pore morphology changes considerably in going from the surface to inner regions of a sample. So (Fig. 25), on the surface dominated by hafnium dioxide, large (5–50 μm) pores prevail. At the same time, vertically extended pores occur in various areas of the oxidized layer, which likely served for gas evolution in the course of plasma chemical exposure. At the boundary with the silicon carbide depleted area, there are horizontally extended pores which can in future serve for the exfoliation of the oxidized portion of the sample (for the reason that the silicon carbide depleted area of the ceramic sample is very porous).

Table 3 lists the thicknesses of oxidized areas for all of the samples studied. One can see that the behavior under similar parameters of exposure to dissociated air streams and the thickness of the oxidized area vary depending on the composition of the HfB_2-SiC ceramic composite sample. When a sample is arranged with a protrusion of ~1.5 mm, the anodic supply power of the plasmatron changes stepwise, and then the pressure increases, the samples having the minimal SiC percentage (10 vol %; sample 10V-1), start rapidly cooling at a higher power (64 kW), and when the pressure increases to 120–130 hPa. For samples of set 2 (15 vol % SiC: sample 15V-1), a rapid rise in surface temperature is observed under milder exposure: the power is also 64 kW and the pressure is lower (110–120 hPa). With this, the maximal surface temperature for samples of sets 1 and 2 is attained at temperatures higher than 2700°C, which is close to the melting temperature of the highest melting component of the oxidized layer (HfO_2, $T_m = 2780 \pm 30$ [33] or 2820 [34]); oxidized

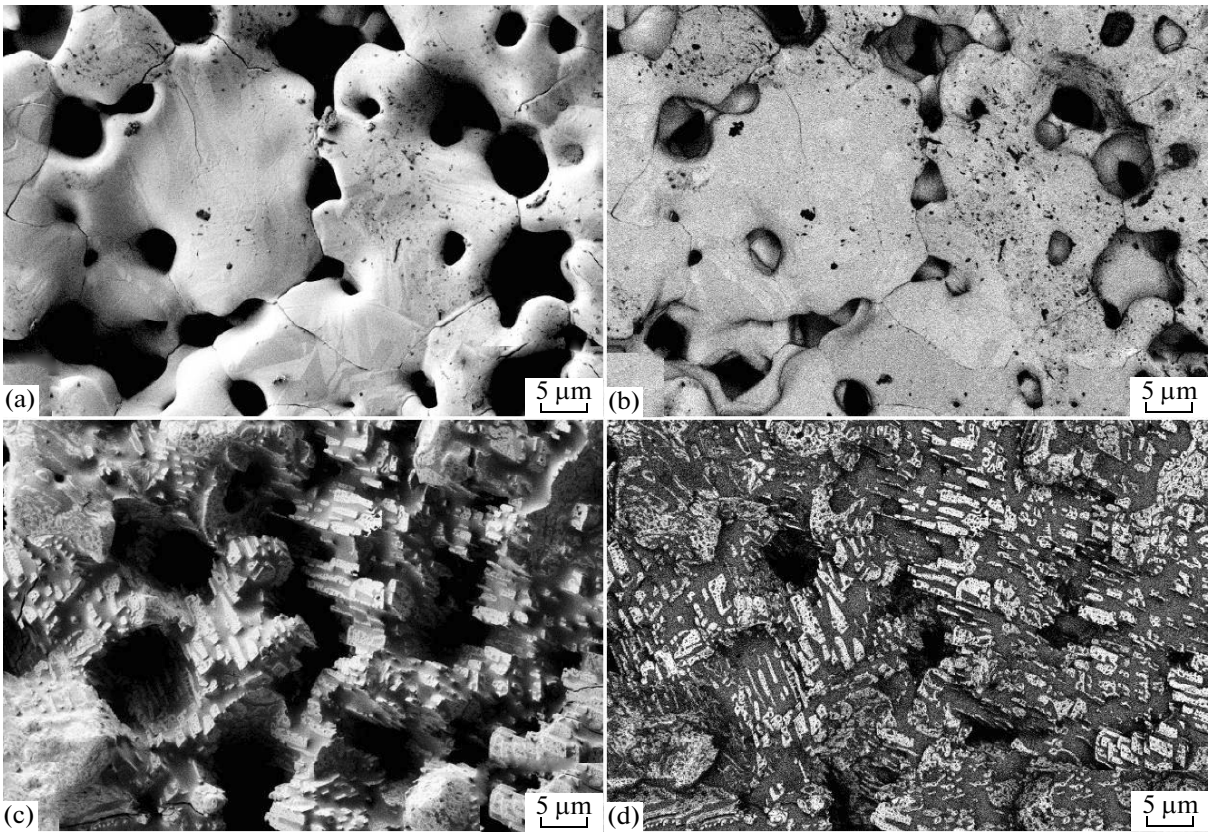

Fig. 22. Surface microstructure of sample 20V-2 of set 3 after exposure to dissociated air flows (as probed by SEM): (a, c) surface morphology as probed by a secondary electron detector for (a) hot area and (c) cold area and (b, d) in the atomic number averaged contrast mode.

layers for these samples have roughly equal thicknesses. The samples of set 3 containing 20 vol % silicon carbide (sample 20V-1 and sample 20V-2) are distinguished by a very rapid increase in temperature under molder exposure conditions even at the least power (45 kW) and a pressure of 110 hPa. The maximal surface temperature for these samples does not exceed 2600–2610°C, which is lower than for samples of sets 1 and 2, so that both the maximal and average thicknesses of the oxidized portion are 200–300 μm smaller. Pressure in the course of the experiment is also of importance because both the oxygen concentration and the activity of evaporation of volatile boron and silicon oxides are pressure dependent, and this can be manifested in the weight change of the sample after tests.

On the whole we may say that, regardless of the composition and porosity, all samples withstood exposure to dissociated air streams without being disintegrated, despite the high temperature attained (2600–2740°C). Rapid cooling when heating was switched off (by more than 1500°C in 3–5 s) likewise did not gave rise to cracking or bundling immediately after the tests. An HfO_2 thermal barrier surface layer was observed for all samples (on the area heated to 2600–2700°C). On the areas where the temperature did not exceed 1800–1900°C, there were mixtures of HfO_2 (a refractory skeleton: solid pillars) and hafnone, which

Table 3. Thicknesses l of oxidized regions (omitting SiC-depleted layers) for HfB_2-SiC ceramic material samples after exposure to dissociated air streams

Sample no.	l_{max}, μm	l_{min}, μm	l_{avg}, μm*
Set 1 (10 vol % SiC)			
10V-1	390	30**	140–180
10V-2	934	480	700–900
Set 2 (15 vol % SiC)			
15V-1	950	375	650–900
15V-2	980	340	700–900
Set 3 (20 vol % SiC)			
20V-1	710	120**	400–650
20V-2***	720	160**	300–600

* In the hot area.

** In the cold area.

*** The oxidized portion of sample 20V-2 cleaved from the region depleted of silicon carbide during section preparation.

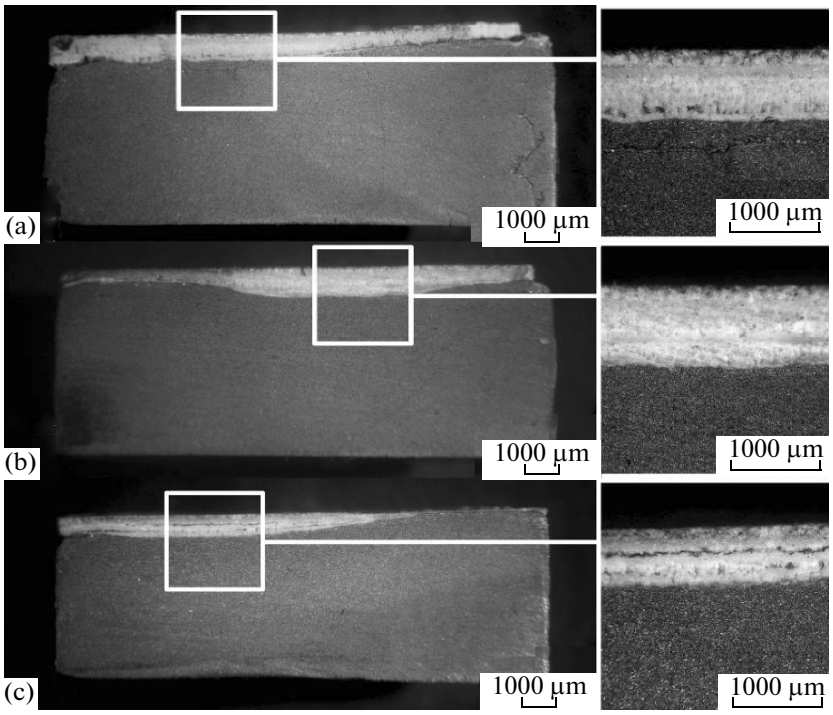

Fig. 23. Sectional microstructures of samples as probed by optical microscopy: (a) sample 10V-2, (b) sample 15V-1, and (c) 20V-1.

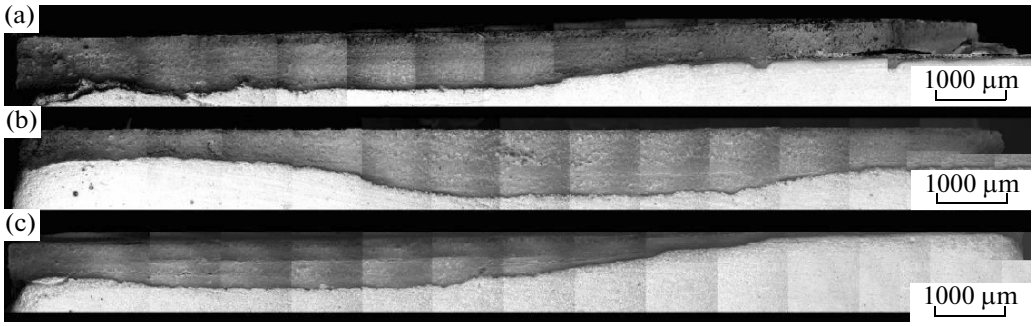

Fig. 24. Sectional microstructures of samples as probed by SEM (InLens secondary electron detector): (a) sample 10V-2, (b) sample 15V-1, and (c) sample 20V-1.

crystallized from the low-boron-oxide borosilicate glass melt; that glass was extruded to the surface under an excess pressure of silicon and carbon monoxides (liquid roof) and actively evaporated to progressively open glass-wetted pores of HfO_2 solid pillars because of the high temperature of the liquid roof and a relatively low pressure in the high-pressure chamber of the plasmatron. These phenomena are also intrinsic to samples with higher silicon carbide percentages (25, 35, and 45 vol %); the results obtained by exposure of those samples to dissociated air streams have been described earlier [6, 7].

CONCLUSIONS

We employed spark plasma sintering to manufacture HfB_2-SiC ultra-high-temperature composite materials having diverse silicon carbide volume percentages (10, 15, and 20 vol %) and the tailored porosities of ~35–40%. We have not observed significant

Fig. 25. Sectional microstructure of sample 10V-2 (hot area) as probed by SEM (SE2 secondary electron detector).

defects on the surfaces of samples; the arithmetic mean deviation of the profile derived from surface roughness was ~1.5–2.0 μm. The elemental and phase compositions of the materials have been determined.

HfB_2-SiC ceramic composite samples were exposed to high-enthalpy dissociated air streams of a VGU-4 induction plasmatron with an anode supply power of 45 to 72 kW and a pressure of 100 to 200 hPa in the plasmatron high-pressure chamber. Under certain parameters of the experiment (which were appreciably differentiated for samples of different sets), local overheating areas were observed to appear (as a rule, the temperature at the edges of the sample considerably exceeded 2000°C); these areas progressively merged during exposure to dissociated air streams to occupy the entire or almost entire surface area of the sample. The temperature acquired values of 2550–2600 (in samples containing 20 vol % SiC) or 2700–2740°C (in samples containing 10 or 15 vol % SiC). We have shown that samples that experienced exposure to temperatures of 2600–2700 and those exposed to 1800–1900°C differed appreciably from one another in the phase and elemental compositions and in surface and cross sectional microstructures.

Our studies prove the potential of HfB_2-SiC porous materials manufactured using spark plasma sintering for use under heating, in particular, under exposure to dissociated air flows at ultrahigh surface temperatures and prove the need for continuing systematic research in this field.

ACKNOWLEDGMENTS

This study was supported by the Presidential Grant for young scientists (MK-1435.2013.3) and the Russian Foundation for Basic Research (13-03-12206-ofi_m).

REFERENCES

1. E. P. Simonenko, D. V. Sevast'yanov, and N.P. Simonenko et al., Russ. J. Inorg. Chem. **58**, 1669 (2013).
2. M. M. Opeka, I. G. Talmy, and J. A. Zaykoski, J. Mater. Sci. **39**, 5887 (2004).
3. F. Monteverde and R. Savino, J. Am. Ceram. Soc. **95**, 2282 (2012).
4. T. H. Squire and J. Marschall, J. Eur. Ceram. Soc. **30**, 2239 (2010).
5. W. G. Fahrenholtz and G. E. Hilmas, Int. Mater. Rev. **57** (1), 61 (2012).
6. V. G. Sevast'yanov, E. P. Simonenko and A. N. Gordeev, et al., Russ. J. Inorg. Chem. **58**, 1269 (2013).
7. V.G. Sevastyanov, E. P. Simonenko and A. N. Gordeev, et al., Russ. J. Inorg. Chem. **59**, 1298 (2014).
8. J. Marschall, D. A. Pejaković, W. G. Fahrenholtz, et al., J. Thermophys. Heat Transfer **26**, 559 (2012).
9. M. Gasch, D. Ellerby, E. Irby, et al., J. Mater. Sci. **39**, 5925 (2004).
10. X. Jin, R. He, X. Zhang, et al., J. Alloys Compd. **566**, 125 (2013).
11. J. B. Berkowitz-Mattuck, Tech. Rep. ASDTDR-62-203, AFML, WPAFB, OH, 1962/1963.
12. F. Monteverde, R. Savino, and M. Fumo, Corros. Sci. **53**, 922 (2011).
13. F. Monteverde, R. Savino, M. Fumo, et al., J. Eur. Ceram. Soc. **30**, 2313 (2010).
14. M. Gasch and S. Johnson, J. Eur. Ceram. Soc. **30**, 2337 (2010).
15. D. Sciti and L. Silvestroni, J. Eur. Ceram. Soc. **32**, 1933 (2012).
16. D. Sciti, R. Savino, and L. Silvestroni, J. Eur. Ceram. Soc. **32**, 1837 (2012).
17. J. Zou, G.-J. Zhang, C.-F. Hub, et al., J. Eur. Ceram. Soc. **32**, 2519 (2012).
18. L. Silvestroni and D. Sciti, J. Eur. Ceram. Soc. **33**, 403 (2013).
19. M. W. Bird, R. P. Aunea, F. Yu, et al., J. Eur. Ceram. Soc. **33**, 2407 (2013).
20. J. Zou, G.-J. Zhang, J. Vleugels, and O. Van der Biestba, J. Eur. Ceram. Soc. **33**, 1609 (2013).

21. S. Gangireddy, J. W. Halloran, and Z. N. Wing, J. Eur. Ceram. Soc. **33**, 2901 (2013).
22. W. Tan, C. A. Petorak, and R. W. Trice, J. Eur. Ceram. Soc. **34**, 1 (2014).
23. C. Carney, A. Paul, S. Venugopal, et al., J. Eur. Ceram. Soc. **34**, 1045 (2014).
24. M. Tului, B. Giambi, S. Lionetti, et al., Surf. Coat. Technol. **207**, 182 (2012).
25. P. A. Williams, R. Sakidj, J. H. Perepezko, and P. Ritt, J. Eur. Ceram. Soc. **32**, 3875 (2012).
26. A. N. Gordeev and A. F. Kolesnikov, *Challenging Topics of Mechanics: Physicochemical Mechanics of Liquids and Gases* (Nauka, Moscow, 2010) [in Russian].
27. D. E. Wiley, W. R. Manning, and O. Hunter, Jr., J. Less-Common Met. **18**, 149 (1969).
28. T. Kawamura, Miner. J. (Japan) **4**, 333 (1965).
29. J. Li, T. J. Lenosky, C. J. Foörst, et al., J. Am. Ceram. Soc. **91**, 1475 (2008).
30. T. A. Parthasarathy, R. A. Rapp, M. Opeka, et al., J. Am. Ceram. Soc. **95**, 338 (2012).
31. W. G. Fahrenholtz, J. Am. Ceram. Soc. **90**, 143 (2007).
32. V. N. Parfenenkov, R. G. Grebenshchikov, and N. A. Toropov, Dokl. Akad. Nauk SSSR **185**, 840 (1969).
33. *Thermodynamic Properties of Materials*, Ed. by V. P. Glushko (Nauka, Moscow, 1978–1982), Vols. 1–4 [in Russian].
34. A. V. Shevchenko, L. M. Lopato, V. D. Tkachenko, and A. K. Ruban, Inorg. Mater. **23**, 225 (1987).

Translated by O. Fedorova